geosciences

MDPI

Article

Holocene Paleoenvironmental Implications of Diatom, Non-Pollen Palynomorph, and Organic Carbon Records from the Kandalaksha Bay of the White Sea (European Arctic)

Yelena Polyakova [1], Elizaveta Agafonova [2,*], Ekaterina Novichkova [2] and Anne de Vernal [3]

[1] Geographical Faculty, Lomonosov Moscow State University, Moscow 119991, Russia
[2] Shirshov Institute of Oceanology, Russian Academy of Sciences, Moscow 119991, Russia
[3] Geotop Research Center in Earth System Dynamics, Université du Québec à Montréal, Montréal, QC H3C3P8, Canada
* Correspondence: agafonovaelizaveta@mail.ru

Abstract: Variations in sea surface conditions and sea level through the Holocene in the Kandalaksha Bay, the White Sea, were reconstructed based on the study of core sediments from the outer Kandalaksha Bay, using the modern analog technique applied to dinocysts in addition to diatoms, TOC, $\delta^{13}C_{org}$, $CaCO_3$, and grain size data. The chronostratigraphy of the core sediments was defined from accelerator mass spectrometry ^{14}C dates on mollusk shells. The results indicated an increase in water depth in the outer Kandalaksha Bay and in the central Dvina Bay until the late Holocene. From about 9.5 to 7.5 cal kyr BP, the data suggested a general trend of increasing sea surface temperatures (up to 14 °C), at least in areas with inflow of Atlantic waters. The last 2.5 kyr were characterized by increased freshwater runoff to the White Sea.

Keywords: the European Arctic; the White Sea; diatoms; dinocysts; Holocene; paleoenvironments

Citation: Polyakova, Y.; Agafonova, E.; Novichkova, E.; de Vernal, A. Holocene Paleoenvironmental Implications of Diatom, Non-Pollen Palynomorph, and Organic Carbon Records from the Kandalaksha Bay of the White Sea (European Arctic). *Geosciences* **2023**, *13*, 56. https://doi.org/10.3390/geosciences13020056

Academic Editors: Leopold Lobkovsky and Jesus Martinez-Frias

Received: 11 November 2022
Revised: 3 February 2023
Accepted: 6 February 2023
Published: 11 February 2023

1. Introduction

The amplified response to the recent global climate change in the Arctic that has been widely documented relates to increased heat transfer from the North Atlantic, atmospheric and surface ocean temperature rise, and reduction of the sea ice cover [1–6]. Therefore, it is particularly relevant to study past and ongoing changes in Arctic marine ecosystems and to reconstruct the variations with the aim to understand and quantify the natural environmental variability and to predict its further evolution under anthropogenic stresses.

The White Sea belongs to the Arctic Ocean as a small and isolated water body (Figure 1a). Its hydrological regime is primarily governed by the inflow of the Barents Sea waters, which are formed from both the Arctic water mass flowing from the north and the Atlantic waters entering the Arctic Ocean from the southwest via the North Atlantic Current (NAC). In the southwestern Barents Sea, the NAC is divided into two main branches: the West Spitsbergen Current turning north along the continental slope and the North Cape stream heading into the Barents Sea (Figure 1a,b). Therefore, the transformed Barents Sea waters entering the White Sea contain an oceanographic signal from the North Atlantic [7–10].

After the last glacial maximum, the ice retreat in the White Sea area occurred between 17 and 12.7 cal kyr BP [11–13]. Exchange with the Barents Sea started 11.7 to 11.2 cal kyr BP [14], when the global sea level reached the depth of the Gorlo Strait sill at 40–42 m below the present-day sea level [15–19].

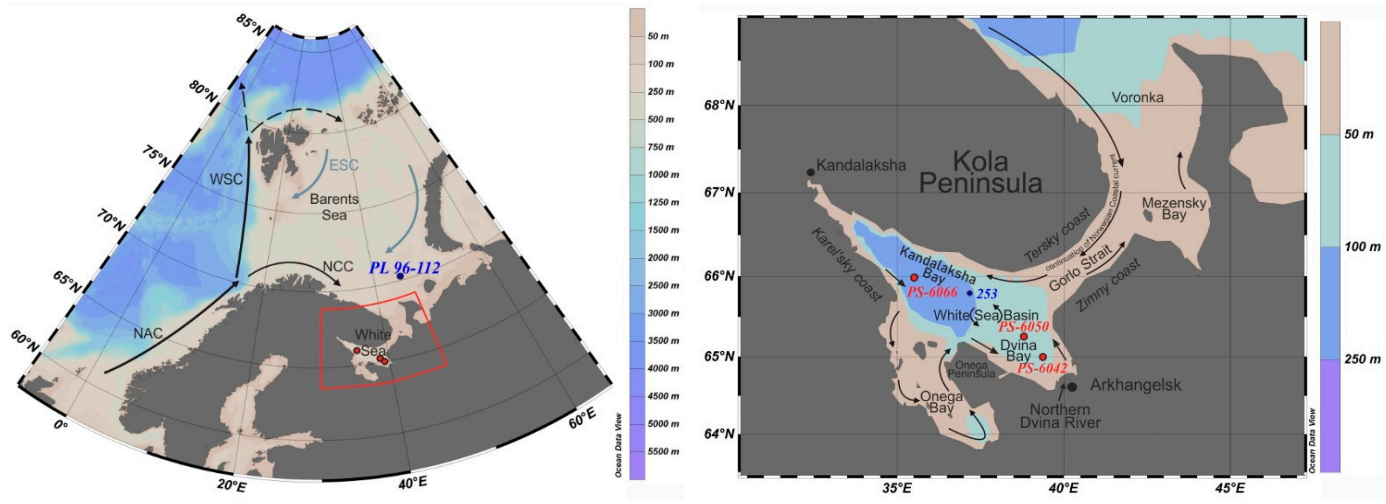

(**a**) (**b**)

Figure 1. Map showing the locations of the studied cores and modern surface currents in the North Atlantic (**a**) and the White Sea (**b**). Arrows indicate the direction of surface currents: ESC—East Spitsbergen Current; WSC—West Spitsbergen Current; NAC—North Atlantic Current; NCC—Norwegian Coastal Current. Sediment core sites from this and previous studies are indicated by red and blue circles, respectively: Core 253 [20], PS-6050, PS-6042 by [21,22], and PL 96-112 by [23].

Despite several research projects conducted on White Sea sediment cores [20,24–27], the chronostratigraphy of the area remained poorly defined due to low content in biogenic carbonate remains in Holocene sequences making it difficult to obtain the ^{14}C date. The rare dates obtained through accelerator mass spectrometry (AMS) ^{14}C measurements were published in our previous studies [21,28].

Here we present new paleoenvironmental data based on the analyses of the sediment core PS-6066, in which an age model based on new AMS ^{14}C dates was defined. The core PS-6066 was collected in the Kandalaksha Bay, the deepest estuary in the White Sea that reaches a maximum water depth of 343 m [29]. Our aim was to reconstruct the sea surface salinity and temperature, seasonal sea ice cover, and other environmental parameters based on multiproxy records. These included micropaleontological tracers (diatoms and dinocysts), in addition to lithological and geochemical properties (grain size, $CaCO_3$ and organic carbon concentration, and δ^{13}C of organic carbon) of the sediment. Diatom and non-pollen palynomorph (NPP) assemblages are among the most useful micropaleontological groups for paleoenvironmental reconstructions in the White Sea region [20–22,30–33]. Diatoms dominate in the phytoplankton communities [34–38], and dinoflagellates are very important components of the White Sea ecosystem. Our interpretations of fossil assemblages of diatoms and NPP in core sediments were based primarily on the previously established patterns of their distribution in the surface sediments and their relationship with hydrological and sedimentation processes [21,31,32,39,40]. We used the modern analog technique [41,42] for the reconstruction of the salinity, temperature, and duration of the sea ice cover.

2. Modern Setting

The White Sea is the most enclosed part of the Eurasian sector of the Arctic Ocean and is almost entirely located south of the polar circle. The origin of the White Sea basin is associated with the development of a rift system that arose in the Middle–Late Riphean on the Early Precambrian consolidated basement [43]. The configuration of the modern basin and the physiography of the surrounding areas have formed under the Neogene–Quaternary tectonic and Quaternary glacial activity [11,44].

The average seawater depth of the White Sea is about 67 m. The maximum depths are recorded in the central depression named the Basin (down to 350 m water depth) and in the Kandalaksha Bay, where it reaches 343 m [29]. With respect to the structure and geomorphology, the following major structural elements are distinguished: the Voronka, the Gorlo, the Basin, and the bays of Onega, Dvina, Mezensky, and Kandalaksha, into which large rivers of the same name flow (Figure 1b). These bays differ in the freshwater supply, amplitude of tides, salinity gradients, sea ice conditions, and biota [45–48].

The present-day hydrology of the White Sea is mostly under the influence of the freshwater runoff, water exchange with the Barents Sea, and strong tidal currents. Freshwater runoff is carried out mainly by the largest rivers, the Dvina, Mezen, Onega, and others, the total flow of which exceeds 225 km^3/year, which defines the regularities and particular features of the hydrological and biogeochemical processes within its area [7,29,46]. Tides in the White Sea reach their maximal heights of up to 7.7 m in the Mezensky Bay and up to 1.6 m in the Dvina Bay, while they do not exceed 2.5 m in the Kandalaksha Bay. Under the conditions of extensive shallow waters in bays, tides have a profound impact on the mixing of water masses in the White Sea.

Water masses entering the White Sea from the Barents Sea have an Atlantic origin [7,10]. They are characterized by a consistently high salinity of 34–35 psu and a relatively high temperature (Figure 2a,b) as compared with other Arctic seas. The surface water temperatures in the White Sea range from +7 to +15 °C in summer and fall down to a freezing point below −1.6 °C in winter [29]. There is a general cyclonic circulation in the sea, homogenizing the water masses. The hydrographic system is characterized by uniform currents due to the continental runoff, concentrated in the upstream part of the bays. In the outer Dvina Bay, the cold deep-sea layers are much closer to the surface than in other parts of the basin. The temperature of 0 °C is observed here in summer only 12–15 m below the water surface. The existence of this unique "hydrological pole of cold" [49] is due to the cyclonic circulation of surface waters with deep-water upwelling in the center.

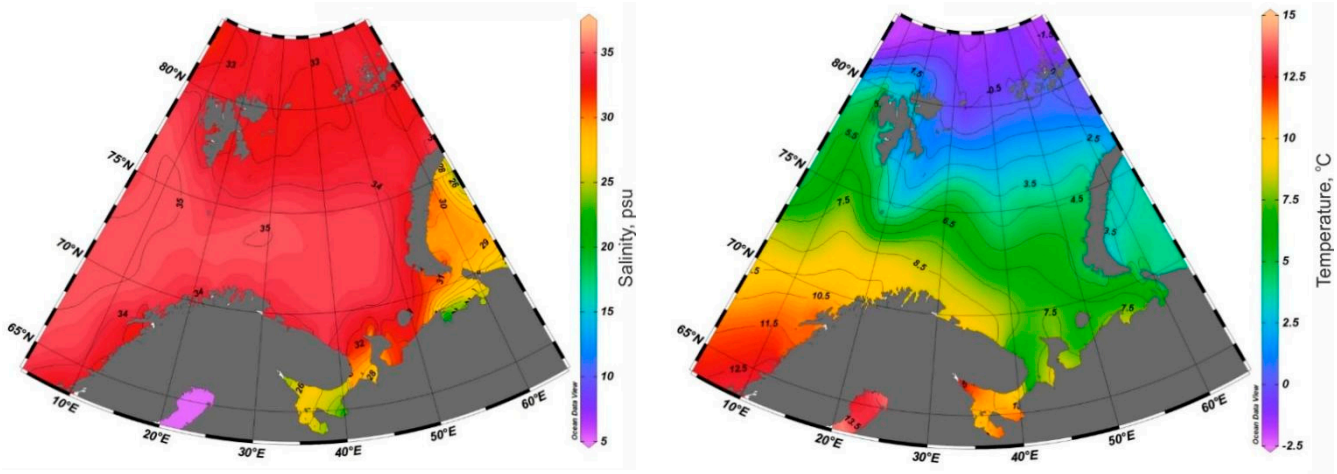

(**a**) (**b**)

Figure 2. Map of mean summer (**a**) sea surface salinity and (**b**) temperature in the White and Barents Seas between 1955 and 2012, after the World Ocean Atlas [50,51].

3. Material and Methods

3.1. Core Location and Processing

The gravity core PS-6066 (65°59.691′ N, 35°32,387′ E; water depth, 266 m) was collected in the Kandalaksha Bay (Figure 1a,b), the NW White Sea, during the R/V *Professor Shtokman* Cruise 80 in 2006. The core was sampled at 1 cm intervals, and the sediment samples were placed in plastic boxes and stored in a cold room (<5° C) until freeze-drying.

3.2. Lithology and Grain Size Analysis

The grain size analysis was carried out at 10 cm intervals using the Petelin method (wet-sieving method combined with the pipette method) [52,53], which is based on Stokes' law. The grain size classification of sediments was reported according to Bezrukov-Lisitzin [54] as follows: gravel (10–1 mm), sand (1–0.1 mm), silt (0.1–0.01 mm), and pelite (<0.01 mm).

3.3. Organic Matter Analysis

The total organic carbon (TOC) content was determined by the automatic coulometric method using an AN7529M Carbon Analyzer M (GZIP, Gomel, Republic of Belarus) that yielded results with an accuracy of ±0.1%. The $CaCO_3$ content was calculated from inorganic carbon with a coefficient of 8.33 according to molar ratio. The results were given in weight percent (wt.%).

The $\delta^{13}C_{org}$ was determined from carbon dioxide obtained through the burning of the samples previously treated with hydrochloric acid to remove carbonate compounds. The $\delta^{13}C$ was measured using a Delta Plus mass spectrometer (Thermo Electron Corporation, Germany) at the Winogradov Institute of Microbiology, Russian Academy of Sciences, Federal Research Centre "Fundamentals of Biotechnology" of the Russian Academy of Sciences. The reproducibility was better than ±0.1‰ for $\delta^{13}C$. The results were presented as $\delta^{13}C$ versus the international standard Vienna Pee Dee Belemnite (VPDB).

3.4. Chronology and Sedimentation Rates

Two AMS ^{14}C dates on bivalves and brachiopods were obtained from the core PS-6066 (Table 1) and calibrated to calendar ages using the Bacon software [55] and the Marine 20 calibration data set that included corrections for the air–sea reservoir difference [56]. We further applied a delta R of −132 ± 48.0 yr calculated using the method of Bevington [57] and the regional data reported in Zaretskaya et al. [58]. In the White Sea, Zaretskaya et al. [58] obtained marine reservoir values ranging from 435 to 535 ^{14}C years for mollusks inhabiting depths of 20–30 m, thus practically leveled out by the correction for isotopic fractionation. The authors, however, mentioned that some mollusks inhabiting deeper than 30–40 m settings may record much larger reservoir effects [58].

Table 1. Accelerator mass spectrometry (AMS) ^{14}C dates and calibrated ages from core PS-6066. Lab codes: Poz—Poznań Radiocarbon Laboratory.

Lab ID	Sample Depth, cm	Dated Material	^{14}C Date	ΔR	Calibrated Age Range ± 1σ	Age, cal yr BP (Median Probability)
Poz-54698	38–39	Shell debris	1930 ± 40	−132 ± 48.0	1260–1630	1545
Poz-66019	221–222	Shell debris	10,290 ± 60	−132 ± 48.0	11,091–11,889	11,490

It should be noted that the White Sea sediments do not contain much material for dating, most of the foraminifer shells being agglutinated. Because carbonate material could not be recovered in the 39−211 cm interval from core PS-6066, we tried to constrain the chronology from correlations with the lithology of the previously studied core PS-6050 [22]. On this basis, we set an interpolated age (see also Section 4.1. Lithology) that was added in the Bacon input file to generate a depth–age model as illustrated in Figure 3.

The ages are given hereafter in cal kyr BP (thousands of calendar years before 1950 CE). The estimated age–depth relationship suggested that average sedimentation rates in the Kandalaksha Bay were about 18–20 cm yr^{-1}, with maximum values of up to 27 cm yr^{-1} for the last ~1.5 cal kyr BP (Figure 3). Thus, the sedimentation rates seemed mostly uniform, which was consistent with continuous marine sedimentation during the Holocene.

The age model allowed us to make ecostratigraphical correlations based on diatom eco-zones and pollen and spore assemblages of other cores from the White Sea area [20,21,25,28]. The uncertainties in the absolute ages are larger than 200 years, as is often the case in marine sequences of subarctic settings [59,60].

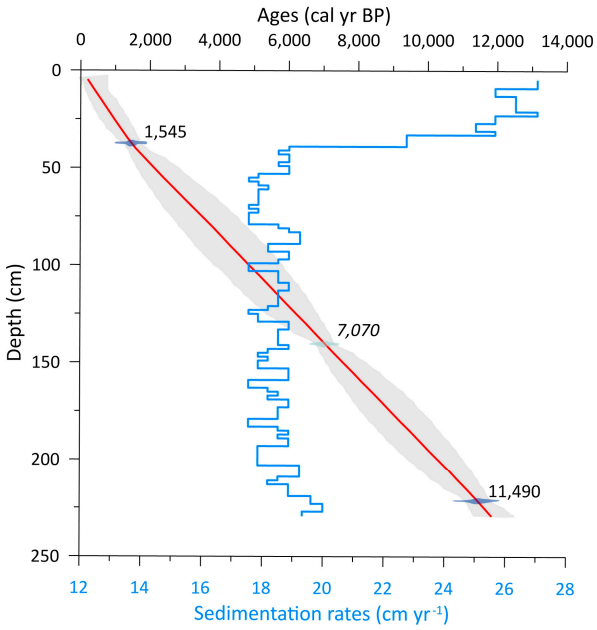

Figure 3. Age–depth model for core PS-6066 constrained from the Bacon software [55] to calibrated accelerator mass spectrometry ^{14}C dates from Table 1. Numbers are the calibrated ages (yr BP), and the one in italics is the added age from interpolation with PS-6050.

3.5. Diatom Study

The diatom assemblages from the core PS-6066 sediments were analyzed in 32 sediment samples. The samples were first freeze-dried, then treated with 30% H_2O_2, concentrated by decantation using distilled water [61], and mounted on slides with Naphrax media (refractive index of 1.74) at the IO RAS. A total of 300–400 specimens were counted in each sample, using an Axiostar Plus microscope (Carl Zeiss, Germany) (oil immersion CP-Apochromat lens, magnification 1000×, numerical aperture 1.25). Diatom identification was carried out at the species, variety, or form levels. The diatom total concentrations per gram of dry sediment (valves/g) were calculated using the Battarbee method [62]. The ecological characteristics of species were from several sources, including the Identification Book of Freshwater Algae of the USSR [63], Diatoms of the USSR [61,64,65], Diatoms of Russia and Adjacent Countries [66,67], Algae [68], Hartley et al. [69], Krammer [70,71], Lange-Bertalot [72], Polyakova [73], Barinova et al. [74], Guiry and Guiry, AlgaeBase [75], Diatoms of North America [76], etc. For the paleoenvironmental reconstructions, the diatom species were grouped into several ecological groups based on their habitat, salinity tolerance, distribution, and phytogeography (Table S1).

The diatoms were first divided according to habitat as planktonic, benthic, meroplanktonic, and periphytic (including epipelic, epiphytic, and epipsammic) species [77]. They were also distinguished based on salinity tolerance as marine (polyhaline), brackish (mesohaline), and freshwater (oligohaline) [78–80]. Following Jousé [81], Semina [82], and Il'yash [37], the planktonic marine diatoms were further subdivided into neritic species, panthalassic species (living in both shelf and ocean zones), and oceanic species. The latter are extremely rare in plankton and sediments of the White Sea [20,37,39]. The White Sea, like other Eurasian Arctic seas, is characterized by extensive shallow-water shelves characterized by specific assemblages of diatoms [32,73,83–85]. These diatom assemblages include planktonic neritic species but also taxonomically diverse benthic and periphytic species, as well as meroplanktonic species, part of the life cycle of which occurs in the form of fouling usually higher aquatic plants.

We also used the classification of phytogeographical groups developed by Beklemishev and Semina [86], with some clarifications of the species affiliation [34,87]. The diatom species were further divided into the following phytogeographical groups: cosmopoli-

tan, boreal, arcto-boreal, and bipolar. Among the neritic and panthalassic species, we distinguished relatively warm-water species such as *Coscinodiscus radiatus, C. perforatus, Shionodiscus oestrupii*, *Actinoptychus senarius*, and others, which were all indicators of Atlantic Water advection into the Arctic seas [84–86]. Particular attention was paid to the sea ice species; *Attheya septentrionalis, Melosira arctica*, and *Nitzschia frigida*, among others, are associated with sea ice at least for a part of their life cycle [85,88,89]. We also noted the presence of ice-neritic species, which developed in the phytoplankton of the marginal ice zone, at low surface water temperatures close to or below 0 °C, such as *Porosira glacialis*, *Thalassiosira nordenskioeldii*, *Bacterosira bathyomphala*, *Rhizosolenia hebetata* f. *hebetata*, and *Chaetoceros furcellatus* [85,89–92].

The freshwater diatom genera *Aulacoseira* and *Cyclotella* and green algae appeared on the shelf with a riverine outflow, and most of them were deposited within the coagulation–sorption stage of the marginal filter of rivers [32,73,93].

According to the change in total diatom concentration in sediments, taxonomic diversity, and distribution of the main ecological groups, as well as the dominant and subdominant taxa, five diatom ecozones (DZ) were distinguished.

3.6. Non-Pollen Palynomorphs, "Pollen and Spores" Studies

Marine dinoflagellate cysts (dinocysts) and other non-pollen palynomorphs (mainly freshwater green algae, acritarchs, and foraminifer organic linings) as well as pollen and spores were studied in 34 samples using a standard palynological technique [32,94]. The sediment samples were treated with cold 10% HCl for 1 h to remove carbonates and with cold 48% HF for 5−10 days to remove siliceous particles. The residue was rinsed twice with distilled water and centrifuged after each step. The samples were then sonicated for 0.2 and 0.8 min and sieved through 15 μm mesh sieves to eliminate pelite. No oxidation was conducted to prevent the loss of the more fragile *Protoperidinium* cysts [95]. A total of 100–300 dinocysts were identified in each slide using an Axiostar Plus microscope (Carl Zeiss, magnification 400× or 1000×) following the nomenclature provided in the literature [96–100]. Pollen grains and spores were counted to quantify inputs from land vegetation using Kupriyanova and Aleshina [101,102] Kupriyanova [103], and Reille [104]. Pollen and spores of terrestrial plants in the bottom sediments of the White Sea related to inputs from river runoff and aeolian transport [25]. NPP, pollen, and spore concentrations were calculated based on the marker grain method using tablets of *Lycopodium clavatum* spores, cf. Stockmarr [105].

Special attention was paid to dinocyst assemblages as the percentages of the dinocyst taxa were determined for reconstructions of past sea surface conditions. The dinocyst assemblages were related to a combination of hydrographic parameters, among which sea surface temperature (SST), sea surface salinity (SSS), sea ice, and productivity appeared the most determinant [106,107]. We used the modern analog technique (MAT) [41,106,107] to quantitatively reconstruct the SST (°C) and SSS (PSU) in winter and summer, sea ice cover (months yr^{-1} > 50%), and primary productivity ($gC/m^2\ yr^{-1}$). The reconstructions were based on the dinocyst reference database updated in 2020 [42,107] that includes data from 1968 sites documenting the modern distribution of dinocysts and a wide range of hydrographical conditions (Table S2). The reconstructions were created from the five best modern analogs as identified from the distance (inversely proportional to the similarity) calculated after log-transformation of percentage data. In the case of the n = 1968 database, the threshold distance for good analogs was 1.2 [107].

4. Results

4.1. Lithology and Organic Matter Content in Core PS-6066

In core PS-6066, which encompassed the entire Holocene according to the AMS ^{14}C ages (Table 1 and Figure 3), the sediments consisted of olive-gray silty pelite (2.42–1.40 m), dark olive silty pelite (1.40–0.04 m), and dark brown clayey silt (0.04–0.00 m) (Figure 4). The upper unit of core PS-6066 (1.40–0 m) correlated with the 2.20–0 m interval in core PS-6050,

which both showed distinct boundaries from grayish sediments to olive sediments dated at about 7.0 cal kyr BP in core PS-6050 [22].

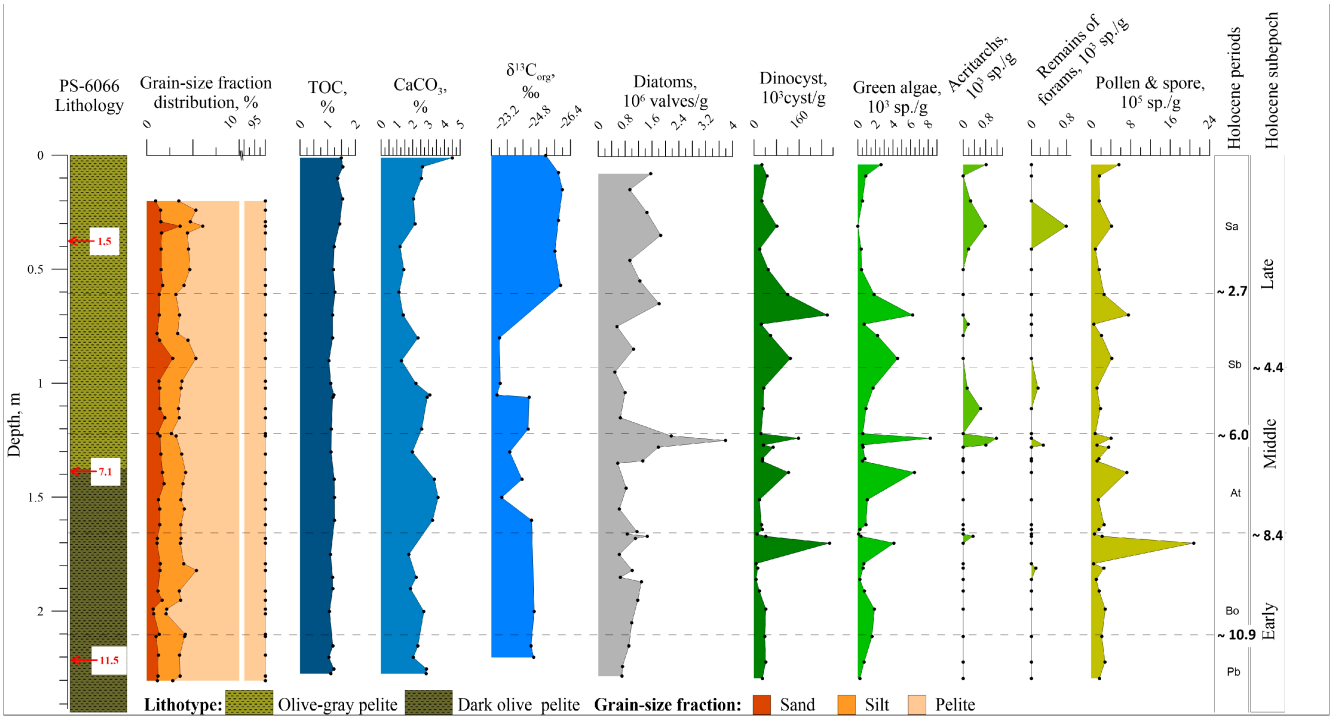

Figure 4. Lithological units; grain size; total organic carbon; calcium carbonate; carbon isotope composition of organic carbon, marked in blue; concentrations of diatoms, marked in gray; dinocysts; green algae; acritarchs; organic foraminifera linings; and pollen and spores (marked in green) expressed in the number of specimens per gram of sediment in core PS-6066, the Kandalaksha Bay. The age model dates in cal kyr BP are marked in red, and the boundary dates in cal kyr BP are black.

According to the results of the grain size analysis, pelite (>95%) dominated the sequence (Figure 4). The sand content varied between 0.6 and 3.9% with abundance peaks at 195, 89, and 31 cm.

The proportions of organic carbon in the core sediments ranged from 1 to 1.5%, while they varied in surface sediments from 0 in the Gorlo Strait to 3.07% in the deep-water part of the White Sea [108]. The $\delta^{13}C_{org}$ suggested changes in the nature of organic fluxes. From 2.42 to 1.60 m, $\delta^{13}C_{org}$ ranged from –24.41 to –24.57‰, which is typical of coastal marine sediments with high terrestrial material inputs. From 1.60 to 0.60 m, the $\delta^{13}C_{org}$ increased to values ranging between –24.31 and −22.68‰, indicating a decrease in terrestrial input relative to marine fluxes. The upper part of the core was characterized by lower $\delta^{13}C_{org}$, down to –26‰, suggesting a high proportion of organic matter from a terrestrial origin [109].

The $CaCO_3$ varied between 1.1 and 4.5%, which corresponded to the contents in the surface sediments of about 1–5% in the central part of the White Sea [24].

4.2. Diatom Assemblages in Core PS-6066

In core PS-6066, the concentration of diatoms was high and varied from 0.49×10^6 to 3.79×10^6 valves/g. The overall taxonomic diversity of diatoms in the assemblages reached 81 taxa, among which 17 were freshwater and 64 were marine or brackish. The marine diatoms dominated (89–100%), with abundant planktonic neritic and panthalassic species. The percentage of panthalassic taxa that increased significantly toward the top of the core (from 29 to 87%) indicated an increase in water depth in the outer Kandalaksha Bay. *Coscinodiscus radiatus*, which is an indicator of Atlantic waters in the western Arctic seas [83–85], was a common panthalassic species of the assemblages. Marine sublittoral

diatoms were mostly represented by the meroplanktonic *Paralia sulcata*, typical for the fouling of higher aquatic plants in the White Sea [110,111]. The abundance of *Paralia sulcata* was maximal in the lower part of the core, reaching up to 54%, and gradually decreased by half up core, confirming an increase in water depth. It was also worth noting the occurrence of freshwater diatoms in core sediments (0.008–0.124 × 10^6 valves/g). The proportions of the freshwater species (*Aulacoseira ambigua*, *Cyclotella meneghiniana*, *Stephanodiscus neoastrea*, etc.) commonly transported to the shelf seas with river runoff varied from 1 to 8%. The main sources of riverine diatoms in the study area were the Varzuga and Umba rivers, along with numerous streams draining the Tersky and Karel'sky coasts. In the core, six diatom assemblage ecozones (DZ) were distinguished based on changes in the ecological affinities of taxa and the composition of dominant and subdominant species (Figure 5).

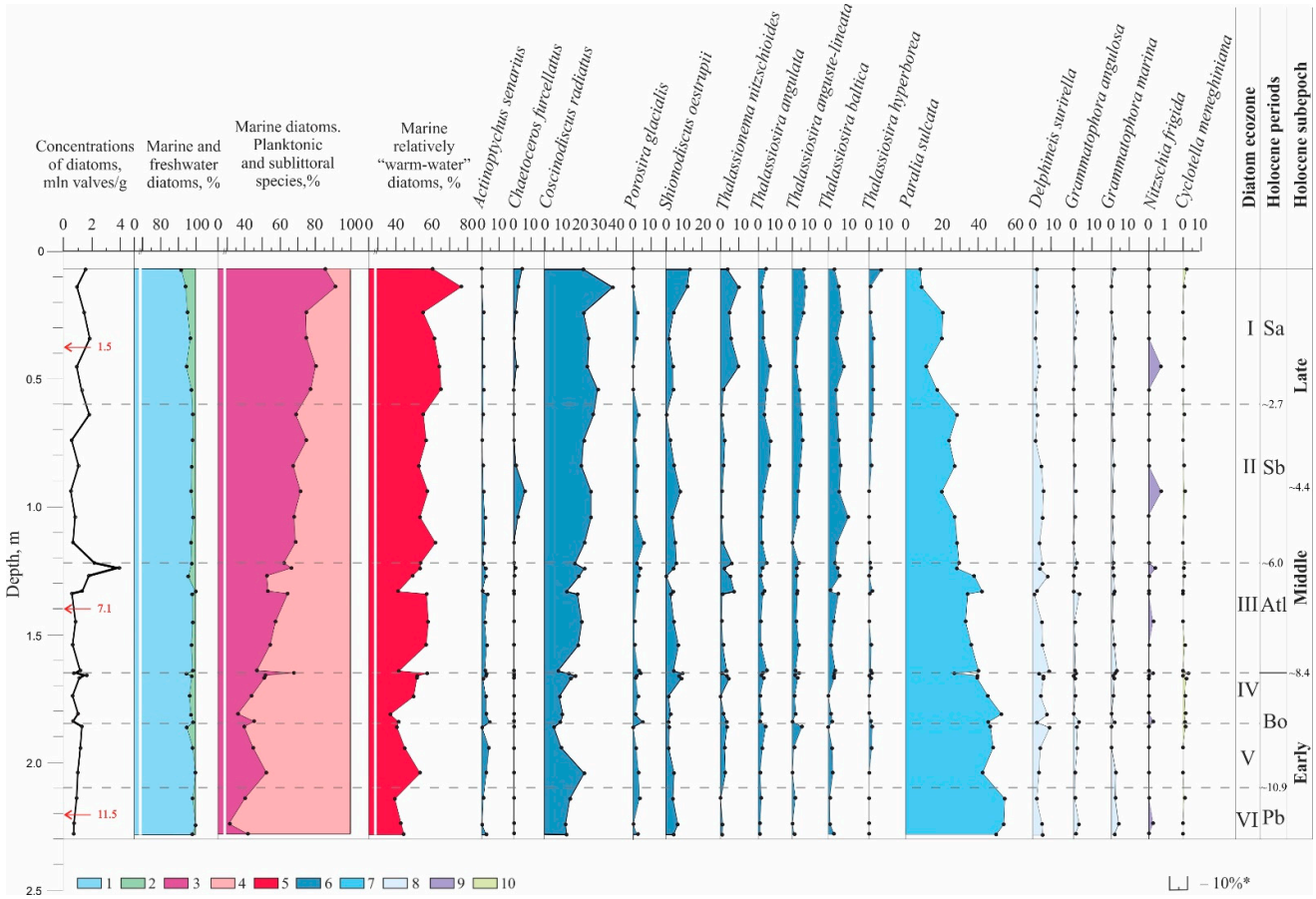

Figure 5. Diatom concentration and percentage of the main taxa in core PS-6066. 1—marine diatoms; 2—freshwater diatoms; 3—marine planktonic diatoms; 4—marine sublittoral diatoms; 5—relatively "warm-water" marine diatoms; 6—plankton neritic and pantalassic taxa; 7—meroplanktonic taxa; 8—sublittoral benthic taxa and periphyton; 9—sea ice taxa; 10—freshwater taxa. Diatom percentage ticks are 10%, except for *Nitzschia frigida* (1%). The dates in cal kyr BP are indicated in red in the diatom concentration column. The Holocene stages and diatom ecozones are indicated in the right margin. Age boundaries from the correlations are in black.

DZ VI (2.28–2.10 m, ~11.7–10.9 cal kyr BP) corresponded to the Preboreal. The concentrations of diatoms in the olive-gray pelite at the base of core were low and did not exceed 0.9 × 10^6 valves/g. DZ VI was characterized by the dominance (62–70%) of sublittoral species (*Delphineis surirella*, *Grammatophora hamulifera*, and *G. marina*), with maximum meroplanktonic Paralia sulcata (up to 54%). Most of the marine planktonic neritic diatoms were represented by relatively warm-water species (*Coscinodiscus radiatus*,

C. perforatus, and *Shionodiscus oestrupii*; up to 32%), indicating advection of Atlantic waters in the Kandalaksha Bay.

DZ V (2.10–1.85 m) from the olive-gray pelite corresponded to the beginning of the Boreal (ca. 10.9–9.5 cal kyr BP). The concentrations of diatoms slightly increased but did not exceed 1.3×10^6 valves/g. The marine sublittoral diatoms remained predominant (up to 62%) with a high proportion of the meroplanktonic species *Paralia sulcata* (up to 48%). The abundances of the Atlantic water species such as *Shionodiscus oestrupii*, *Coscinodiscus radiatus*, *C. perforatus*, and *Actinoptychus senarius* increased up to 42%.

DZ IV (1.85–1.65 m, olive-gray pelite), which likely corresponded to the second half of the Boreal (9.5–8.4 cal kyr BP), was characterized by concentrations of diatoms varying slightly (0.6–1.4 $\times 10^6$ valves/g). The percentage of *Coscinodiscus radiatus* decreased significantly (down to 8%), while sublittoral meroplanktonic species (*Paralia sulcata, Delphineis surirella*, etc.) increased up to 68%, and the single sea ice *Nitzschia frigida* appeared in the lower part of the layer. The number of warm-water planktonic diatoms, indicators of Atlantic waters including *Coscinodiscus radiatus*, increased upward (from 30 to 43%).

DZ III (1.65–1.22 m, 8.4–6.0 cal kyr BP, olive-gray pelite) was marked in its lower part (1.65–1.34 m, 8.4–6.7 cal kyr BP) by a low number of diatoms (0.58–1.1 $\times 10^6$ valves/g). The diatom assemblages of DZ III were significantly enriched (up to 50%) in relatively warm-water species, including the Atlantic water taxa *Actinoptychus senarius, Coscinodiscus radiatus*, and *Shionodiscus oestrupii* [83–85]. In the upper part of the zone (ca. 6.7–6.0 cal kyr BP) the abundance of diatoms sharply increased (1.3–3.8 $\times 10^6$ valves/g), with the occurrence of the sublittoral meroplanktonic species *Paralia sulcata* and *Delphineis surirella*. Furthermore, the neritic cold-water species *Porosira gracialis, Bacterosira bathyomphala*, and *Rhizosolenia hebetata* f. *hebetata* slightly increased. The sea ice *Nitzschia frigida* and ice-neritic species *Chaetoceros furcellatus* also occurred.

DZ II (1.22–0.60 m, 6.0–2.7 cal kyr BP, dark-olive pelite) corresponded to the Subboreal, according to the age model. It was characterized by low diatom concentrations (1.0–0.5 $\times 10^6$ valves/g), which slightly increased upward in the core (up to 1.8 $\times 10^6$ valves/g). There was a gradual decline in the abundances of sublittoral diatoms, notably the meroplanktonic species *Paralia sulcata* and *Delphineis surirella* (from 34 to 20%). Likewise, in the group of marine planktonic diatoms, there was a general increase in relative abundances (from 22 to 27%) of Coscinodiscus radiatus, except a short interval of 0.94–0.84 m (ca. 4.5–4.0 cal kyr BP). In the lower part of the layer (1.22–0.84 m; ca. 6.0–4.0 cal kyr BP), the occurrence of the cold-water species *Chaetoceros furcellatus, Porosira gracialis*, and *Bacterosira bathyomphala* increased (up to 5%), and the sea ice species *Attheya septentrionalis, Melosira arctica*, and *Nitzschia frigida* were notable.

DZ I (0.60–0.00 m, ca. 2.7 cal kyr BP to the present) from the dark olive pelite in the uppermost part of core corresponded to the Subatlantic. The concentration of diatoms varied from 0.9 to 1.8 $\times 10^6$ valves/g. The relative abundance of dominant marine neritic species increased up to 73%, most of them being represented by planktonic species indicative of Atlantic water such as *Coscinodiscus radiatus, Shionodiscus oestrupii*, and *Thalassiosira anguste-lineata* (57%). The concentration of sublittoral diatoms decreased to 27%. In the lower part of the layer (0.60–0.34 m, ca. 2.7–1.3 cal kyr BP), the sea ice species *Attheya septentrionalis, Melosira arctica*, and *Nitzschia frigida* occurred. The abundance of freshwater species, planktonic (*Aulacoseira subarctica* and *Cyclotella meneghiniana*), benthic (*Cocconeis pediculus*), and periphytic (*Diploneis elliptica*, *Epithemia sorex*, etc.) increased up to 8%, which suggested enhanced freshwater discharge from the Varzuga River.

4.3. Palynomorph Assemblages in Core PS-6066

In the modern sediments of the White Sea and Barents Sea, the influence of Atlantic water masses is marked by the occurrence of the phototrophic dinocyst species, *Operculodinium centrocarpum* [32]. Assemblages with common *O. centrocarpum* are typical of the western shelf edge of the Barents Sea and West Spitsbergen [112,113], as well as of the White Sea [32]. *Islandinium minutum* subsp. *minutum* often dominate in sediments of areas

marked by Arctic surface waters mass distribution area, together with other heterotrophic taxa, notably *Brigantedinium* spp. [112,113] in the Barents Sea, and *Echinidinium karaense* and *Selenopemphix quanta* in the White Sea [32].

Micropaleontological analysis in core PS-6066 showed the presence of common palynomorphs, including dinoflagellate cysts (dinocyst), freshwater green algae, acritarchs, foraminifer organic linings, pollen grains, and spores. The most abundant palynomorphs were dinocysts (up to 271 $\times$ 10^3 cysts/g), pollen and spores of terrestrial plants (up to ~2 $\times$ 10^6 grains/g), and green algae (up to 7.4 $\times$ 10^3 sp./g). Dinocysts were represented in the core by 14 taxa. In general, cosmopolitan species such as *O. centrocarpum* were associated with the penetration of Atlantic waters [114,115]. The palynomorphs concentrations, percentages of the main dinocyst taxa, and grain size led to the definition of three main assemblage zones in the PS-6066 core (Figure 6).

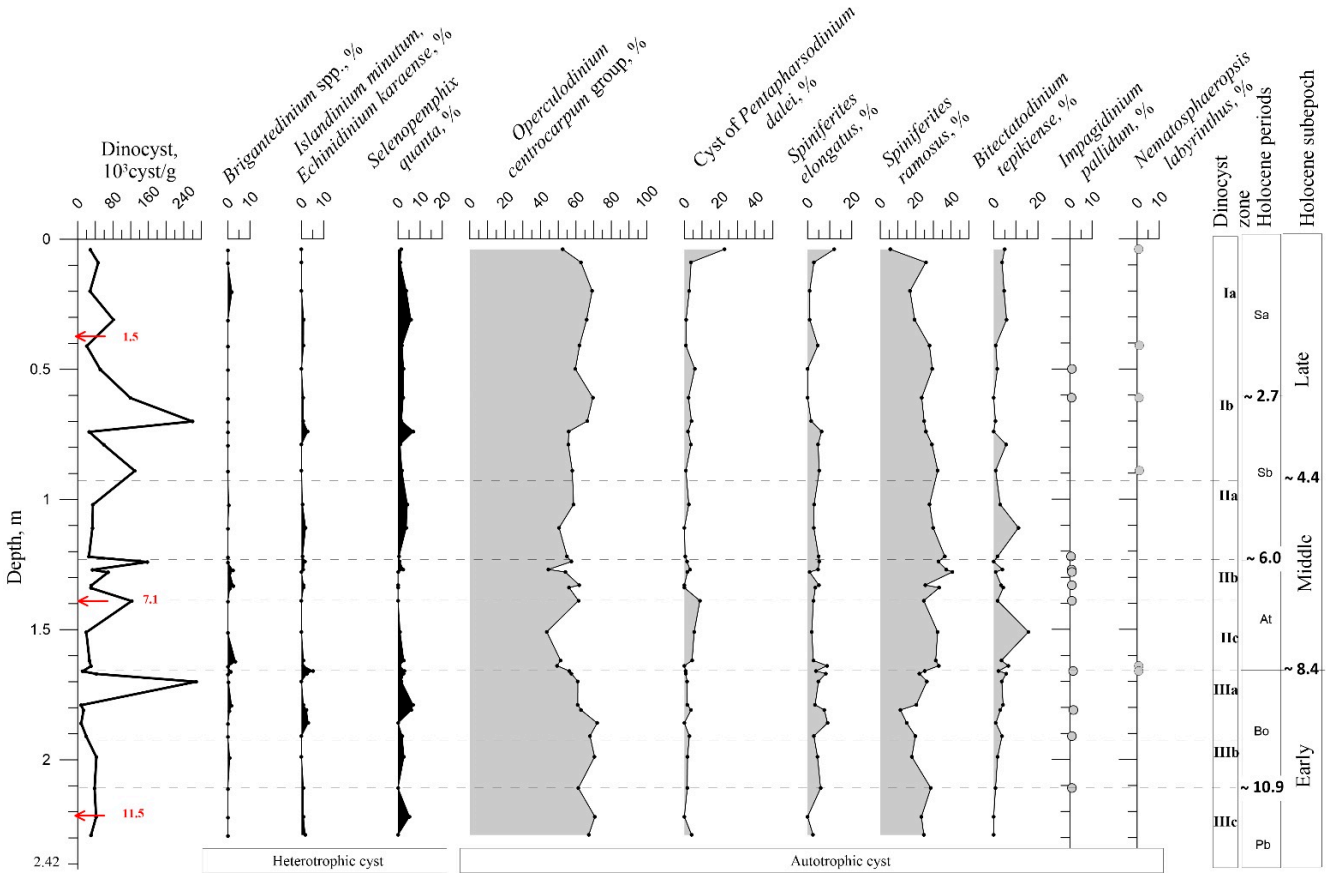

Figure 6. Dinocyst concentrations and relative abundance (percentages of the main taxa in core PS-6066. Dark gray and light gray mark heterotrophic and autotrophic species, respectively. The Holocene stages and dinocyst ecozones are marked on the right. Age model dates in cal kyr BP are marked in red, and boundary dates in cal kyr BP are in black.

Zone III at the base of the core (2.42–1.65 m; 11.7–8.4 cal kyr BP) was subdivided into three subzones. Subzone IIIc (2.42–2.10 m; 11.7–10.9 cal kyr BP) was characterized by the dominance of *Operculodinium centrocarpum* that includes various morphological types (up to 71%) and *Spiniferites* spp. (up to 23%). The heterotrophic species *Selenopemphix quanta*, *Islandinium minutum* subsp. *minutum*, and *Echinidinium karaense* do not exceed 6.9%. Dinocyst concentrations are 30–42 $\times$ 10^3 cysts/g, and the content of freshwater green algae is low, not exceeding 0.7 sp./g. The concentrations of pollen grains and spores were 167–280 $\times$ 10^3 grains/g and were much higher than those of marine NPP (Figure 6).

In subzone IIIb (2.10–1.92 m; 10.9–9.9 cal kyr BP), the species diversity of dinocysts increased, and the Impagidinium pallidum, which is typical for fully marine conditions

with high salinity, appeared singly [116]. At a depth of about 2 m, the sediment became more fine-grained (pelite ~ 98%), but then the sandy fraction reached up to 1.7%.

A slight increase in coarse-grained sediment in subzone IIIa (1.92–1.65 m; 9.9–8.4 cal kyr BP) was accompanied by a sharp short-term increase in heterotrophic species (*I. minutum*, *E. karaense*, *S. quanta*, and *Brigantedinium* spp.) up to 8–10%, although autotrophic cosmopolitan species generally dominated [32]. Heterotrophic dinocysts were associated with an environment with dense seasonal sea ice cover [96,97,106,107]. In addition, the *Nematosphaeropsis labyrinthus* (about 1%), found exclusively in completely marine conditions, was encountered for the first time, and the frequency of the findings of *Impagidinium pallidum* (1–2%) also increased. Further, the concentrations of dinocysts reached up to 270×10^3 cysts/g, and the freshwater green algae (up to 7.4 sp./g) and the pollen and spores (up to 2×10^6 grains/g) sharply increased (Figure 6). Subzone IIIa was characterized also by the diversity of spores and pollen and the predominance of up to 99% of tree species (mainly *Pinus* and *Picea* genus) with single grains of *Betula nana* and *Alnus*. However, it should be noted that there was a sharp maximum in the proportion of *Sphagnum* and *Polypodiaceae* spores (almost up to 4% in total) at the zone boundary at 1.92 m.

Zone II (IIc, 1.65–1.38 m; 8.4–6.9 cal kyr BP) was characterized by a decrease in the proportion of the *O. centrocarpum* species to 42% and was accompanied by an increase in other autotrophic species: *Pentapharsodinium dalei* cysts up to 9% and *Bitectatodinium tepikiense* up to 16%. The presence of the latter two species in modern sediments of the Arctic seas was often associated with low-duration (<4 months a year) sea ice cover, as well as with the passage of the polar front and/or increased productivity [97,116].

Subzone IIb (1.38–1.22 m; 6.9–6 cal kyr BP) was characterized by a slight decrease in the proportion of heterotrophic species down to 2%, while autotrophic species reached their maximum. In addition to the general predominance of cysts of the genus *Operculodinium* (up to 61%), the cysts of *S. ramosus* and *S. elongatus* reached 44% by the end of the period. In addition, almost all samples contained single cysts of *Impagidinium pallidum* up to 1%.

Subzone IIa (1.22–0.92 m; 6–4.4 cal kyr BP) was characterized by increases in the proportion of heterotrophic relatively cold-water species up to 7.5% and was noted especially at a depth of 1.16–1.02 m. In addition, the proportion of the *Operculodinium* cyst, which currently occupies about 50% in the associations, was reduced.

The palynomorph Zone I (Ib, 0.92–0.60 m; 4.4–2.7 cal kyr BP) was marked at its base by an increase in the concentrations of aquatic and terrestrial palynomorphs. The dinocysts content reached a second maximum with values of 260×10^3 cysts/g. The concentrations of green algae and pollen and spores reached 6 and 754×10^3 grains/g, respectively. Toward the top of the zone (Ia, 0.60–0.00 m; 2.7 cal ka BP to the present), the palynomorph concentrations decreased.

In Zone I, the dinocyst assemblages were characterized by high percentages of *Operculodinium centrocarpum* and a decreasing trend of *Spiniferites* spp. Rare cysts of *Nematosphaeropsis labyrinthus* and *Impagidinium pallidum*, which are typical for subpolar environments of the northeast North Atlantic [106,107,117], were recovered.

4.4. Changes in P/B Ratio Values

The P/B ratio (Figure 7) expresses the proportion of diatom valves belonging to planktonic species to the sum vs. benthic and planktonic species [118–120] following Wang et al. [119].

In core PS-6066 from the outer Kandalaksha Bay, the P/B ratio ranges between 0.29 and 0.86, increasing from the base to the top, which suggests deepening of the water depth. The increase in the P/B ratio from 0.29 to 0.63 occurred before 5.0 cal kyr BP. Two low P/B value peaks (0.62 and 0.60) at about 8.4 and 6.8 cal kyr BP were noted.

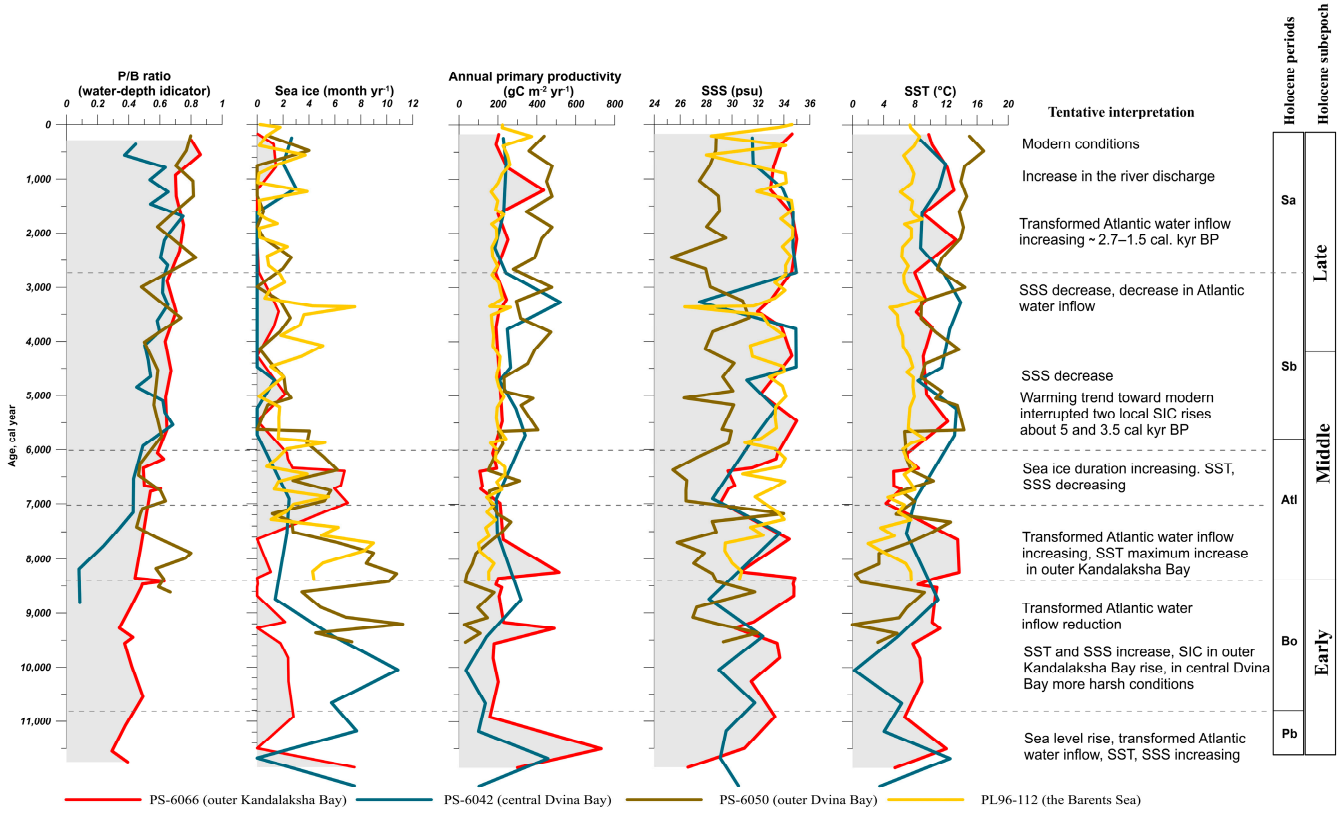

Figure 7. Diatom P/B ratio and quantitative estimates of sea surface parameters in the White Sea (this study) in and the Barents Sea (PL 96-112 by [23]). The Kandalaksha Bay is additionally highlighted by gray.

We calculated the P/B ratios from the data of the previously studied cores PS-6050 and PS-6042 (Figures 1b and 7) collected in the outer and central Dvina Bay, at 101 and 61 meters of water depth, respectively [21,22,28]. The P/B ratio of core PS-6050 showed a trend from 0.3 to 0.8 over the past 8.6 cal kyr BP, which also suggested a temporary increase in water depth in the outer Dvina Bay. Core PS-6042, from the central part of the Dvina Bay, differed significantly from the deep-water areas of the White Sea (Figure 7). The P/B ratio increased from 8.8 to 1.5 cal kyr BP, with the most pronounced change occurring from 8.6 to 5.6 cal kyr BP. The last 1.6 kyr was, however, marked by a decrease in the P/B ratio by almost half, which could have been due to local changes in the water depths most likely caused by local block movements in the Dvinsky graben.

4.5. Reconstruction of Sea Surface Water Conditions

The sea surface conditions were estimated based on the modern analog technique (MAT) using the n = 1968 dinocyst database [42,109] that was applied to assemblages of cores PS-6066 (this study), PS-6042, and PS-6050 [21,22,28]. The distance between fossil and modern analogs mostly varied between 0.3 and 0.6 and never exceeded 0.9 for the first analog, which indicated good modern analogs exist for most samples. The MAT results showed the variation of hydrographic parameters in time and space (Figure 7).

From >11.4 to ~9.5 cal kyr BP, we reconstructed the harsh conditions in the central Dvina Bay with the sea ice cover of 8–10 months yr^{-1}, summer SST of 2–8 °C, and SSS fluctuating between 27 and 32 PSU. At the deepest site of the Kandalaksha Bay, the sea surface conditions were less severe with 4–6 months yr^{-1} of sea ice cover, SSS around 30 PSU, and SST 8–10 °C (Figure 7). From 9.5 to ~7 cal kyr BP a warming trend was reconstructed. The outer part of the Kandalaksha Bay became almost free of sea ice, and the central Dvina Bay recorded the minimum sea ice (~2 months yr^{-1}), while SST reached the maximum of 12–14 °C, and the annual primary productivity increased up

to 500 gC $m^{-2}yr^{-1}$. In the second half of the Middle Holocene at 7–6 cal kyr BP, there was an increase in the duration of seasonal ice cover and a decrease in SSS (to 28–30 PSU) and SST (to about 8 °C). After 6 cal kyr BP, there were few fluctuations in the sea surface parameters. The last notable change in surface water occurred at about 3.5 cal kyr BP when SSS decreased to 28 PSU in the central Dvina Bay, and SST increased up to 2–3 °C. Around 0.5 cal kyr BP, high temperatures were reconstructed in Kandalaksha and the outer part of Dvina Bay (up to 14–16 °C), while they were 2–4 degrees lower in the central Dvina Bay (Figure 7).

It should be noted that the milder conditions in the Kandalaksha Bay than in the Dvina Bay may be associated with the transformed Atlantic water distributions that flow into the Kandalaksha Bay along the Tersky Coast, prior to reaching the Dvina Bay, thus resulting in local particularity in the "hydrological pole of cold" and the "hydrological thermal pole".

5. Discussion

5.1. Holocene Sea Level Changes in the White Sea Area

Reconstruction of the sea level in the White Sea area during the Holocene is a complicated task since the factors that operate in this region include eustatic sea level rise, glacio-isostatic uplift, and regional neotectonic movements. During the last glacial maximum around 21,000 years ago, the global sea level was >120 m lower than at present [12,16–18,121–124]. The average rates of eustatic sea level rise (SLR) were uneven [15,18,125]. From 16.5 to ~8.2 cal kyr BP, it was about 12 mm yr^{-1} with faster rates of ~40 mm yr^{-1} at ~14.5–14.0 cal kyr BP and 11.3 cal kyr BP and slower rates during the Younger Dryas, 12.5–11.5 cal kyr BP [18,19]. The modern eustatic sea level was reached by the end of the Middle Holocene [15,18].

Elevated shorelines evidence isostatic uplift along the White Sea coasts, notably along the Kandalaksha Bay at altitudes up to 100 meters [14,126–129] and in the Dvina Bay at 5−20 m above the present sea level [129]. The discrepancy in the elevation of the shorelines results from the glacioisostatic processes [14,127–132]. Our records from the outer Kandalaksha Bay indicated local deepening of the water depth since the beginning of the Preboreal. The evidence came from the consistent increase in planktonic diatoms from 29 to 87% in core PS-6066 (Figure 5) relative to the decrease in sublittoral diatoms as indicated by the P/B ratio increasing from 0.29 to 0.86 (Figure 7). The record of core PS-6066 was consistent with data from the central White Sea [20] (Figure 1b, core 253) and the inner part of the Kandalaksha Bay [14,128,129].

The deepening of the White Sea was primarily caused by eustatic sea level rise, which was about 50 meters between 11.7 and 5 cal kyr BP [15]. However, the diatom data suggested that the basin deepening continued until recently, which points to neotectonics as the leading factor. The Kandalaksha graben of the White Sea is one of the most active tectonic zones of the eastern part of the Fennoscandian crystal shield. This is confirmed by a system of Holocene active faults, earthquake, and paleoseismic dislocations [133,134].

The Dvina Bay is located within the southeastern tip of the Kandalaksha–Dvinsky Rift, which extends in a northwesterly direction from the Kandalaksha Bay through the central part of the White Sea to the Dvina Bay. It is assumed that this rift experienced continuous subsidence during the Holocene.

Previous diatom investigations of the Dvina Bay sediments [21,22] indicated a gradual increase in marine planktonic taxa. It increased from 29 to 80%, and the P/B ratio increased (from 0.3 to 0.8, Figure 7) toward the top of core PS-6050 from the outer Dvina Bay, indicating deepening over the past 8.6 cal kyr BP [21]. Similarly, in the sediments of the central part of the Dvina Bay (core PS-6042), the planktonic diatoms consistently increased from 9% to 79%, and the proportion of marine sublittoral species decreased from 91 to 21% [22]. From these data, we may conclude that the water depth of the Dvina Bay increased in its outer part and at least until past 1.6 cal kyr in its central part.

The decrease in the P/B ratio in the central Dvina Bay sediments since about 1500 years ago might be caused by decreased water depths locally, which could be due to local tectonic

block movements [135,136]. A decreased bathymetry in the central Dvina Bay during the middle of the Subatlantic was also evidenced by the formation of the Northern Dvina River delta at about 2 cal kyr BP and by coastal ridges on the nearby islands [137].

Our records indicated that while the coasts of the Kandalaksha Bay continued to uplift in the Holocene, the deep-water areas of its outer part and the adjacent Basin, as well as the outer part of the Dvina Bay, experienced sea level rise.

5.2. Holocene Environments in the White Sea

The main environmental changes of the late glacial and postglacial history of the White Sea were related to water exchange with the Barents Sea, which started between 11.7 and 11.2 cal kyr BP [14] when sea level reached about the 40–42 m deep Gorlo Strait sill [11–13].

5.2.1. The Early Holocene Environments. Preboreal and Boreal (~11.7–8.4 cal kyr BP)

According to previous studies, there was permanently a strong current from the Barents Sea, carrying transformed Atlantic waters into the White Sea basin along the Tersky coast to the Kandalaksha Bay (Figure 1b), as at present [11,20].

In the outer Kandalaksha Bay, at the location of core PS 6066, fully marine conditions were already established by the beginning of the Preboreal at ~11.7 cal kyr BP as indicated from diatom (Figure 5) and palynomorph assemblages (Figure 6, subzone IIIc) and $\delta^{13}C_{org}$ values (Figure 4). The dominant sublittoral diatoms and low P/B ratios in the olive-gray pelite with hydrotroilite, however, suggested lower sea level in the outer Kandalaksha Bay than at present (Figure 7).

During the Preboreal, the marine waters of the Kandalaksha Bay penetrated into the land, as evidenced by the abundance of neritic euryhaline diatom species in sediment cores from the upstream part of bay [20,24]. The high abundances of planktonic diatoms in these sediments may indicate the likelihood of high water productivity all over the bay.

The compositions of diatom and aquatic palynomorph assemblages were similar to those recovered near surface sediments (Figures 5 and 6, core PS-6066), which suggested an early onset of modern-like hydrological and hydrobiological conditions. Of particular interest was the confirmation that the penetration of transformed Atlantic waters into the Kandalaksha Bay started at ~11.7 cal kyr BP. The high concentrations and proportions of relatively warm-water planktonic diatoms (*Coscinodiscus radiatus* and *Shionodiscus oestrupii*) and dinocysts (*O. centrocarpum*, cyst of *P. dalei*), which are indicators of Atlantic-sourced waters in the western Arctic [84–86,114,115], proved the wide water exchange between the White and the Barents Seas and the intensive advection of Atlantic waters during the Preboreal. The data led to the inference of an increase in SST, from 2 to 12 °C, and phytoplanktonic productivity up to 730 gC $m^{-2}g^{-1}$.

Our reconstructions are in a good agreement with the diatom and dinocyst data from the northwestern continental slope of the Barents Sea [136]. Based on the records from of the well-dated core SV-04, it was shown that the modern-like conditions characterized by the intensive advection of Atlantic waters were established early during the Holocene (11.2 cal kyr BP) [138].

At the beginning of the Preboreal (~11.7–11.4 cal kyr BP), transformed Atlantic waters also entered the central part of the Dvina Bay, although with lower fluxes as evidenced by diatom and dinocyst of core PS-6042 [22]. Based on low diatom and NPP concentrations, maximum freshwater green algae input, and low $\delta^{13}C_{org}$ (-27.04—28.7), we deduced intensive input of terrigenous organic matter at ~11.7 cal kyr BP into the central Dvina Bay [22,28]. This was consistent with dinocyst data that led to the reconstruction of relatively low salinity (29–30 psu) and productivity (82–457 gC $m^{-2}yr^{-1}$) in the surface waters. This was likely caused by the proximity of study site PS6042 to the Northern Dvina River mouth at a time of lower sea level, by about −40 to −35 m compared with the present [16,139].

During the Boreal (~10.9–8.4 cal kyr BP), a gradual deepening of the outer water depth in the Kandalaksha Bay (PS-6066) was evidenced by a decrease in the relative

abundances of sublittoral diatoms and a rise of the P/B ratios (Figure 7). The species compositions of planktonic diatom and dinocyst assemblages indicated changes in the hydrological conditions.

The first half of the Boreal (Figure 5, ~10.9–9.5 cal kyr BP) was characterized by a slight reduction in the influence of transformed Atlantic waters in the outer Kandalaksha Bay, as inferred from the general decrease in the concentrations of diatoms and dinocysts. An increase in the duration of seasonal sea ice cover (2–4 months yr^{-1}) and a decrease in sea surface temperature (down to 2–8 °C) and annual productivity (100–200 gC $m^{-2}yr^{-1}$) were reconstructed. Nevertheless, the eustatic sea level rise was reflected in the increasing sea surface salinity of the White Sea record. In the second half of the Boreal (~9.2–8.4 cal ka BP), there was a sharp increase in concentrations of palynomorphs in sediments. A shorter duration of seasonal sea ice cover (0–2 months yr^{-1}) may have led to an increase in productivity (189–489 gC $m^{-2}yr^{-1}$) in surface waters. In the outer part of the Kandalaksha Bay, the second half of the Boreal period 9.5–8.4 cal ka BP was marked by an increase in SST and SSS (11–12 °C and 32–34 PSU).

In the central Dvina Bay, core PS 6042 contains sediments dating back to the Boreal period. In the first half of the Boreal (10.9–9.5 cal kyr BP), the sea level rise led to a shift of the Northern Dvina River mouth toward its present position. This was marked by a diminution of the green algae concentrations and changes of $\delta^{13}C_{org}$ to more positive values. Surface water temperatures (0–2 °C) during this period were slightly lower than in the Kandalaksha Bay despite the occurrence of Atlantic water indicator species in the diatom and aquatic palynomorph assemblages. During the second half of the Boreal (9.4–8.2 cal kyr BP), the SST and SSS increased (5–10 °C and 28–32 PSU), and the seasonal sea ice cover decreased (from 5–10 to 1–5 months yr^{-1}).

Sea ice formation in the White Sea starts first at the mouths of bays, where large river fluxes result in low-salinity surface waters, thus fostering early freezing, 1–3 months earlier than more offshore. The extent of seasonal sea ice cover is also governed by wind. By April–May, the "spring bloom" of sea ice diatoms and the active growth of phytoplankton start in the Arctic seas when 50–80% of the sea ice is dispersed to the Barents Sea through the Gorlo Strait by strong winds [29]. The sea ice distribution in the White Sea is reflected in diatom and dinocyst assemblages recovered from bottom sediments as shown from previous studies [31,32,83]. Therefore, we hypothesized that the extensive sea ice and minimal surface water temperatures characterizing the first half of Boreal in the central part of the Dvina Bay were caused by freshening in surface waters due to the relatively close location of the Northern Dvina River mouth [29].

The warming of the end of the Boreal after 9.5 cal kyr BP in the Kandalaksha and Dvina Bays was interrupted by a cooling outer Dvina Bay and outer Kandalaksha Bay (Figure 7). Relatively high percentages of the heterotrophic species *I. minutum* subsp. *minutum* and *E. karaense* suggest more extensive sea ice cover (up to 10 months/year in the outer Dvina Bay) and a decrease in surface water temperatures in the Kandalaksha and Dvina Bays of the White Sea (Figure 7).

5.2.2. The Middle Holocene: Atlantic and the First Half of Subboreal (8.4–4.4 cal kyr BP)

In the first part of Atlantic period (~8.4–7 cal kyr BP) the outer Kandalaksha Bay recorded an increase in SST, up to 14 °C which may coincide with the thermal optimum the Holocene recorded in the Barents Sea to occur from 7.8 ka B.P. to 6.8 ka [140]. This interval was also marked by the deposition of olive-gray pelite in the outer Kandalaksha Bay, the occurrence of relatively warm-water diatom and NNP species (Figure 5), high carbonate content ($CaCO_3$ ~3–4%), and low terrigenous input ($\delta^{13}C_{org}$ ranging from –22.68 to −24.31‰). The SST rise reached its maximum at about 8–7.5 cal kyr BP (Figure 7). In the central Dvina Bay, SST slightly decreased (down to 6–8 °C) during the first half of the Atlantic, whereas it increased from 3 to 12 °C in the outer Dvina Bay.

We hypothesized that higher SST in the Kandalaksha Bay and the outer Dvina Bay in comparison with the central Dvina Bay during the first half of the Atlantic were related to

transformed Atlantic waters entering into the White Sea, first into the Kandalaksha Bay along the Tersky Coast and then into the Dvina Bay. The regional differences may reflect the local structures of the "hydrological pole of cold" and the "hydrological thermal pole". The warming in the Kandalaksha Bay and the outer Dvina Bay is in good agreement with the SST changes in the first half of the Atlantic in the Barents Sea (Figure 7) [23,140].

In the outer Kandalaksha Bay, there was a decrease in SST and SSS (5°C and 29–31 PSU) and productivity (110–193 gC $m^{-2}yr^{-1}$), while sea ice cover extended to 6 months yr^{-1} during the second part of the Atlantic (about 7–5.8 cal kyr BP). Such a mid-Holocene cooling was also recorded in the Barents Sea after 6.7 kyr BP [140]. In the White Sea the cooling was also evidenced from the increasing number of cold-water diatom species *Porosira gracialis*, *Bacterosira bathyomphala*, and *Rhizosolenia hebetata f. hebetata* and the occurrence of the sea ice species *Nitzschia frigida* and *Chaetoceros furcellatus* (Figure 5).

In the outer Dvina Bay, SST, SSS, and productivity decreased down to 6 °C, 25 PSU, and 149 gC $m^{-2}yr^{-1}$, respectively, whereas sea ice cover increased up to 6 months yr^{-1}. In the central Dvina Bay, the conditions remained similar to those of the first half of the Atlantic.

The maximum diatom concentrations in the outer Kandalaksha Bay (core PS-6066, the upper part of DZ III, Figure 5) and in the outer and central Dvina Bay [21,22] occurred at about 6.7–6 cal kyr BP. Thus, the White Sea sediments recorded a maximum concentration of diatoms, which may correspond to a change in the sedimentary regime, as well as an increase in the productivity of diatoms. We interpreted the increased diatoms and NPP concentrations as the result of the input of biophilic trace elements from seasonal sea ice. Apparently, the mechanism of sea ice melt and opening differed from the modern one and was primarily associated with wind-driven upwelling. This was consistent with the occurrence of sea ice and ice-neritic diatom species in the outer Kandalaksha Bay and the Dvina Bay [21,22] sediments. The high Si content could alternatively derive from river discharge and the underground runoff, which increased due to relict permafrost thawing [141].

In the outer Kandalaksha Bay, the beginning of the Subboreal (after ~5.8 cal kyr BP) was marked by increased SST (12 °C) and SSS (34 PSU). In the outer and central Dvina Bay, SST and SSS also increased up to 8–14 and 8–13 °C and up to 34 and 30 PSU, respectively. Nonetheless, the decrease in diatom concentration, the increase in the number of relatively cold-water species, and the occurrence of the diatom sea ice species *Attheya septentrionalis* in the Kandalaksha (Figure 5, ~6–4.4 cal kyr BP) and Dvina Bays [21,22] indicated a cooling in the first half of the Subboreal. We also assumed that the presence of sea ice species in sediments may have been associated with the seasonal sea ice cover boundary's closer position to the central parts of the bays during the growing season. This corresponded well with two high sea ice concentration events (~5 and 3.5 cal kyr BP) from the Kandalaksha Bay.

5.2.3. The Late Holocene: Second Half of the Subboreal and Subatlantic (the Last ~4.4 cal kyr BP)

In the outer Kandalaksha Bay, the dinocyst data indicate the SSS was about 31–34 PSU and SST–8–10 °C during the second half of the Subboreal. In the outer Dvina Bay, SST increased from 8 to 14 °C, whereas in the central Dvina Bay, it decreased from 13 to 8 °C, and SSS reached 31–34 PSU. The slight increase in the number of warm-water species and diatom concentrations in the outer Kandalaksha might have been due to the increase in the intensity of transformed Atlantic waters. After about 3.5 cal kyr BP, there was a decrease in salinity in the study areas, which could be linked with a decrease in Atlantic water fluxes, as also evidenced in the south of the Barents Sea (Figure 7) [23].

At the beginning of the Subatlantic, about 2000 years ago, there was a short-term increase in SSS up to 34 PSU, probably related to an increase in the intensity of transformed Atlantic waters. In the second part of the Subatlantic, after ~2.0 cal kyr BP, a consistent increase in the number of relatively warm-water diatom and dinocyst species was noted in the outer Kandalaksha Bay, outer Dvina Bay, and central Dvina Bay [21,22,28]. SST values increased during the Subatlantic up to 13 °C in the outer Kandalaksha Bay, to 16 °C in the

outer Dvina Bay, and to 11 °C in the central Dvina Bay. The trend toward lower surface temperatures in the outer Dvina Bay that was particularly pronounced after 2.0 cal kyr BP was probably due to upwelling of cold bottom waters.

The increase in freshwater species (up to 8%) in the outer Kandalaksha Bay core (Figure 5, DZ I) was associated with an increase in the river discharge after ~2.0 cal kyr BP, which was also noted in the central Dvina Bay (up to 40%) and the outer Dvina Bay (up to 8%) cores [21,22]. It was also related to the lowering of sea level along the coastline of the Kandalaksha Bay [14,128,129,142,143] that fostered the influence of the distribution of river fresh waters. The freshwater diatom distributions in the Dvina Bay, up to 40% in the central part and 8% in the outer part, were similar to the modern ones in surface sediments [31]. The increase in river surface runoff was also evidenced from the isotopically light $\delta^{13}C_{org}$ of –26‰ in the upper part of core PS-6066 [109], in agreement with studies of the White Sea drainage basin [111,139]. According to the regional physiography and radiocarbon dating, an increase in river runoff accompanied with the formation of new channels was established in the Subatlantic time period [141,144,145].

6. Conclusions

Diatom and palynomorph assemblages from the ^{14}C-dated sediment core PS-6066 provided new information on the postglacial history in the Kandalaksha Bay, the White Sea, over the Holocene. Data indicated a deepening of the Kandalaksha Bay throughout the Holocene.

The penetration of transformed Atlantic waters into the Kandalaksha Bay started at least 11,700 years ago and between ~11.7 and 11.4 cal kyr BP into the central part of the Dvina Bay (core PS-6042). The data also indicated that the highest SST prevailed in the White Sea from 8 to 7.5 cal ka BP.

In the Kandalaksha (PS-6066) and Dvina (PS-6042, PS-6050) Bays, there was a cooling event in the surface waters marked by relatively low temperatures and salinity, a decrease in productivity, and an increase in sea ice for more than 6 months of the year at the end of the middle Holocene at about ~7–5.8 cal kyr BP.

In the central Dvina Bay, a decrease in surface temperatures more pronounced than in the outer Kandalaksha and outer Dvina Bays was recorded after 2.0 cal kyr BP. The upwelling of cold and nutrient-rich bottom waters could be invoked. Furthermore, the increase in the freshwater diatom species in the outer Kandalaksha Bay and the central and outer Dvina Bay could be associated with increasing river discharge after ~2.0–1.0 cal kyr BP.

The overall records of the White Sea evidence the impact of sea level and hydrological changes in sea surface conditions, including sea ice cover and primary productivity. Our local study of Holocene natural changes in the White Sea contributes to a broader understanding of climate change in the Barents Sea region as a whole and will be considered in further research.

Supplementary Materials: The following are available online at https://www.mdpi.com/article/10.3390/geosciences13020056/s1.

Author Contributions: Conceptualization, E.A., E.N. and Y.P.; methodology, E.A., E.N. and A.d.V.; investigation, E.A., E.N. and Y.P.; data curation, E.N.; writing—original draft preparation, E.A., E.N. and Y.P.; writing—review and editing, E.A., E.N., Y.P. and A.d.V.; visualization, E.A. and E.N. All authors have read and agreed to the published version of the manuscript.

Funding: The sedimentological and micropaleontological study was supported by the Russian Science Foundation (project No 21-17-00235). The diatom researches of the Dvina Bay sediments were carried out within the framework of the State Assignments of Ministry of Science and High Education, Russia (Lomonosov Moscow State University, theme no. 121051100135-0). The studies by A. de V are supported by the Natural Sciences and Engineering Council of Canada.

Data Availability Statement: Not applicable.

Acknowledgments: We thank the crew of the R/V "*Shtokman*" and all participants of the 80th cruises for their co-operation, especially A.E. Rybalko for onboard geological work. We also thank the Academician A.P. Lisitzin† for general leadership and scientists from the Laboratory of Physical Geology Researches of the Shirshov Institute of Oceanology RAS for their assistance. We are very grateful to Elena Ivanova for her invaluable advice and consultations on the Barents Sea paleoreconstructions. Finally, we are greatly indebted to anonymous reviewers for their thorough and meticulous efforts toward improving the manuscript.

Conflicts of Interest: The authors declare no conflict of interest.

References

1. Johannessen, O.M.; Bengtsson, L.; Miles, M.W.; Kuzmina, S.I.; Semenov, V.A.; Alekseev, G.V.; Nagyrnyi, A.P.; Zakharov, V.F.; Bobylev, L.P.; Pettersson, L.H.; et al. Arctic climate change: Observed and modeled temperature and sea ice variability. *Tellus* **2004**, *56A*, 328–341. [CrossRef]
2. Johannessen, O.; Bobylev, L.; Shalina, E.; Sandven, S. *Sea Ice in the Arctic Past, Present and Future: Past, Present and Future*; Springer: Berlin/Heidelberg, Germany, 2019; p. 575. [CrossRef]
3. ACIA. *Impacts of a Warming Arctic: Highlights*; Cambridge University Press: Cambridge, UK, 2004; p. 17.
4. Stroeve, J.C.; Holland, M.M.; Meier, W.; Scambos, T.; Serreze, M. Arctic Sea ice decline: Faster than forecast. *Geophys. Res. Lett.* **2007**, *34*, L09501. [CrossRef]
5. Mahoney, A.R.; Barry, R.G.; Smolyanitsky, V.; Fetterer, F. Observed Sea ice extent in the Russian Arctic, 1933–2006. *J. Geophys. Res.* **2008**, *113*, C11005. [CrossRef]
6. Stocker, T.F.; Qin, D.; Plattner, G.-K.; Tignor, M.; Allen, S.K.; Boschung, J.; Nauels, A.; Xia, Y.; Bex, V.; Midgley, P.M. *IPCC: Climate Change 2013: The Physical Science Basis. Contribution of Working Group I to the Fifth Assessment Report of the Intergovernmental Panel on Climate Change*; Cambridge University Press: Cambridge, UK; New York, NY, USA, 2013; p. 1535. [CrossRef]
7. Berger, V.Y.; Naumov, A.D. General features of the White Sea. Morphology, sediments, hydrology, oxygen conditions, nutrients and organic matter. *Ber. Polarforsch.* **2000**, *359*, 3–9.
8. Pantyulin, A.N. Hydrological system of the White Sea. *Oceanology* **2003**, *43*, 1–14.
9. Pantyulin, A.N. Ice cover and ice of the White Sea after the observation data. In *The White Sea System, Volume II: Water Column and Interacting with It Atmosphere, Cryosphere, River Runoff and Biosphere*; Lisitzin, A.P., Nemirovskaya, I.A., Eds.; Scientific World: Moscow, Russia, 2012; pp. 120–132. (In Russian)
10. Oziel, L.; Sirven, J.; Gascard, J.-C. The Barents Sea frontal zones and water masses variability (1980–2011). *Ocean Sci.* **2016**, *12*, 169–184. [CrossRef]
11. Demidov, I.N. Geology and dynamics of the latest period in the formation of the White Sea. In *The White Sea System. Volume I: Natural Environment of the Catchment Area of the White Sea*; Lisitzin, A.P., Nemirovskaya, I.A., Eds.; Scientific World: Moscow, Russia, 2010; pp. 58–76. (In Russian)
12. Hughes, A.L.C.; Gyllencreutz, R.; Lohne, Ø.S.; Mangerud, J.; Svendsen, J.I. The last Eurasian ice sheets—A chronological database and time-slice reconstruction, DATED-1. *Boreas* **2015**, *45*, 1–45. [CrossRef]
13. Stroeven, A.P.; Hättestrand, C.; Kleman, J.; Heyman, J.; Fabel, D.; Fredin, O.; Goodfellow, B.W.; Harbor, J.M.; Jansen, J.D.; Olsen, L.; et al. Deglaciation of Fennoscandia. *Quat. Sci. Rev.* **2016**, *147*, 91–121. [CrossRef]
14. Kolka, V.V.; Evzerov, V.Y.; Möller, J.J.; Korner, G.D. The Late Weichselian and Holocene relative sea-level change and isolation basin stratigraphy at the Umba settlement, southern coast of Kola Peninsula. *Izv. RAN Akad. Nauk USSR Ser. Geogr.* **2013**, *1*, 73–88. (In Russian) [CrossRef]
15. Fairbanks, R.G. A 17.000-year glacio-eustatic sea level record: Influence of glacial melting rates on the Younger Dryas event and deep ocean circulation. *Nature* **1989**, *342*, 637–642. [CrossRef]
16. Bauch, H.A.; Mueller-Lupp, T.; Taldenkova, E.; Spielhagen, R.F.; Kassens, H.; Grootes, P.M.; Thiede, J.; Heinemeier, J.; Petryashov, V.V. Chronology of the Holocene transgression at the North Siberian margin. *Glob. Planet. Change* **2001**, *31*, 125–139. [CrossRef]
17. Klemann, V.; Heim, B.; Bauch, H.; Wetterich, S.; Opel, T. Sea-level evolution of the Laptev Sea and the East Siberian Sea since the last glacial maximum—Impact of glacial isostatic adjustment. *Arktos* **2015**, *1*, 1. [CrossRef]
18. Lambeck, K.; Rouby, H.; Purcell, A.; Sun, Y.; Sambridge, M. Sea level and global ice volumes from the Last Glacial Maximum to the Holocene. *Proc. Natl. Acad. Sci. USA* **2014**, *111*, 15296–15303. [CrossRef]
19. Cronin, T.; O'Regan, M.; Pearce, C.; Gemery, L.; Toomey, M.; Semiletov, I.; Jakobsson, M. Deglacial sea-level history of the East Siberian Sea Margin. *Clim. Past Discuss.* **2017**, *13*, 1097–1110. [CrossRef]
20. Dzhinoridze, R.N. Diatoms from Bottom Sediments of the White Sea in Connection with Its History in the Holocene. Ph.D. Thesis, Academy of Sciences of the USSR, V.L. Komarov Botanical Institute, Leningrad, Russia, 1971; p. 23. (In Russian).
21. Polyakova, Y.I.; Novichkova, Y.A.; Lisitzin, A.P.; Bauch, H.A.; Rybalko, A.Y. Modern Data on the Biostratigraphy and Geochronology of White Sea Sediments. *Dokl. Earth Sci.* **2014**, *454*, 169–174. [CrossRef]
22. Agafonova, E.; Polyakova, Y.; Novichkova, Y. The diatom response to Postglacial environments in the White Sea, the European Arctic. *Mar. Micropaleontol.* **2020**, *161*, 101927. [CrossRef]

23. Voronina, E.; Polyak, L.; de Vernal, A.; Peyron, O. Holocene variations of sea-surface conditions in the Southeastern Barents Sea, reconstructed from dinoflagellate cyst assemblages. *J. Quat. Sci.* **2001**, *16*, 717–726. [CrossRef]
24. Nevesskii, E.N.; Medvedev, V.S.; Kalinenko, V.V. *The White Sea. Sedimentogenesis and History of Development in Holocene*; Nauka: Moscow, Russia, 1977. (In Russian)
25. Malyasova, E.S. *Palynology of Bottom Sediments of the White Sea*; Leningrad State University: Leningrad, USSR, 1976; p. 120. (In Russian)
26. Rybalko, A.E.; Spiridonov, M.A.; Spiridonova, E.A.; Moskalenko, P.E. Quaternary deposits of the Onega Bay and the main features of its paleogeography in the Pleistocene-Holocene. In *Complex Marine Geological and Geophysical Exploration of Inland Seas of the Glacial Shelf*; Spiridonov, M.A., Moskalenko, P.E., Eds.; VSEGEI: Leningrad, USSR, 1987; pp. 38–52. (In Russian)
27. Rybalko, A.E.; Zhuravlev, V.A.; Semenova, L.R.; Tokarev, M.Y. Quaternary deposits of the White Sea and the history of the development of the modern White Sea basin in the Late Pleistocene—Holocene. In *The White Sea System. Volume IV: The Processes of Sedimentation, Geology and History*; Lisitzin, A.P., Shevchenko, V.P., Vorontsova, V.G., Eds.; Scientific World: Moscow, Russia, 2017; pp. 84–127. (In Russian)
28. Novichkova, Y.A.; Reikhard, L.Y.; Lisitzin, A.P.; Rybalko, A.Y.; de Vernal, A. New data on the Holocene evolution of the Dvina Bay (White Sea). *Dokl. Earth Sci.* **2017**, *474*, 607–611. [CrossRef]
29. Pantyulin, A.N. The features of the White Sea physics—Dynamics, structure and water masses. In *The White Sea System. Volume II: Water Column and Interacting with It Atmosphere, Cryosphere, River Runoff and Biosphere*; Lisitzin, A.P., Nemirovskaya, I.A., Eds.; Scientific World: Moscow, Russia, 2012; pp. 309–378. (In Russian)
30. Polyakova, Y.I. Diatom analysis. In *Methods of Paleogeographic Reconstructions*; Kaplin, P.A., Yanina, T.A., Eds.; Geographical Faculty of MSU: Moscow, Russia, 2010; pp. 126–160. (In Russian)
31. Polyakova, Y.I.; Novichkova, Y.A.; Lisitzin, A.P.; Shevchenko, V.P.; Kravchishina, M.D. Diatoms and aquatic palynomorphs in surface sediments of the White Sea bays as indicators of sedimentation in marginal filters of rivers. *Oceanology* **2016**, *56*, 289–300. [CrossRef]
32. Polyakova, Y.I.; Novichkova, Y.A. Diatoms and aquatic palynomorphs in the White Sea sediments as indicators of sedimentation processes and paleoceanography. In *Sedimentation Processes in the White Sea: The White Sea Environment Volume 2 of Handbook of Environmental Chemistry*; Lisitzin, A.P., Demina, L.L., Eds.; Springer: New York, NY, USA, 2018; pp. 10–48.
33. Shilova, O.S. *Holocene Diatoms of Swamps of the Kola Peninsula and the North Eastern Karelia*; MAX Press: Moscow, Russia, 2011; p. 178. (In Russian)
34. Semina, G.I.; Sergeeva, O.M. Planktonic flora and biogeographical characteristics of the White Sea phytoplankton. In *Ecology and Physiology of Animals and Plants of the White Sea*; Gilyarov, M.S., Pertsov, N.A., Eds.; MSU: Moscow, Russia, 1983; pp. 3–17. (In Russian)
35. Rat'kova, T.N. Phytoplankton composition in the White Sea basin in summer-autumn 1998 and 1999. *Ber. Polarforsch.* **2000**, *359*, 97–100.
36. Rat'kova, T.N. The White Sea basin phytoplankton—A review. *Ber. Polarforsch.* **2000**, *359*, 3–29.
37. Il'yash, L.V.; Zhitina, L.S.; Fedorov, V.D. *Phytoplankton of the White Sea*; Yanus-K: Moscow, Russia, 2003; p. 168. (In Russian)
38. Il'yash, L.V.; Rat'kova, T.N.; Radchenko, I.G.; Zhitina, L.S. Phytoplankton of the White Sea. In *The White Sea System. Volume II: Water Column and Interacting with It Atmosphere, Cryosphere, River Runoff and Biosphere*; Lisitzin, A.P., Nemirovskaya, I.A., Eds.; Scientific World: Moscow, Russia, 2012; pp. 605–640. (In Russian)
39. Polyakova, Y.I.; Dzinoridze, R.N.; Novichkova, T.S. Diatoms and Palynomorphs in the White Sea sediments as indicators of Ice and Hydrological conditions. *Oceanology* **2003**, *43*, 144–158.
40. Novichkova, Y.A.; Polyakova, Y.I. Associations of microalgae in bottom sediments of marginal filters areas (White Sea bays). *Dokl. Earth Sci.* **2013**, *449*, 413–417. [CrossRef]
41. Guiot, J.; de Vernal, A. Transfer functions: Methods for quantitative paleoceanography based on microfossils. In *Proxies in Late Cenozoic Paleoceanography*; Hillaire-Marcel, C., de Vernal, A., Eds.; Elsevier Science: Amsterdam, The Netherlands, 2007; pp. 523–563.
42. de Vernal, A.; Hillaire-Marce, C.; Rochon, A.; Fréchette, B.; Henry, M.; Solignac, S.; Bonnet, S. Dinocyst-based reconstructions of sea ice cover concentration during the Holocene in the Arctic Ocean, the northern North Atlantic Ocean and its adjacent seas. *Quat. Sci. Rev.* **2013**, *79*, 111–121. [CrossRef]
43. Baluev, A.S.; Zhuravlev, V.A.; Przhiyalgovskii, E.S. New data on the structure of the central part of the White Sea paleorift system. *Dokl. Earth Sci.* **2009**, *427*, 891–896. [CrossRef]
44. Baluev, A.S.; Zhuravlev, V.A. Geological structure and tectonic evolution of the pre-Quaternary bed of the White Sea and adjacent territories. In *The White Sea System. Volume IV: The Processes of Sedimentation, Geology and History*; Lisitzin, A.P., Shevchenko, V.P., Vorontsova, V.G., Eds.; Scientific World: Moscow, Russia, 2017; pp. 16–84. (In Russian)
45. Lisitzin, A.P.; Shevchenko, V.P.; Burenkov, V.I.; Kopelevich, O.V.; Vasil'ev, L.Y. Suspended matter and hydrooptics of the White Sea: New patterns of quantitative distribution and grainsize analysis. In *Actual Problems of Oceanology*; Laverov, N.P., Ed.; Nauka: Moscow, Russia, 2003; pp. 554–608. (In Russian)
46. Gordeev, V.V. Rivers of Russian Arctic: Flows of sediments from continent to the ocean. *New Ideas Oceanol.* **2004**, *2*, 113–166. (In Russian)

47. Lisitzin, A.P. The processes in the White Sea catchment area: Preparation, transfer and sedimentation of matter, flows of matter, and the concept of "living watershed". In *The White Sea System. Volume I: Natural Environment of the Catchment Area of the White Sea*; Lisitzin, A.P., Nemirovskaya, I.A., Eds.; Scientific World: Moscow, Russia, 2010; pp. 353–445. (In Russian)
48. Lisitzin, A.P. Dispersed sedimentary substance in the earth geospheres and in the White Sea system. In *The White Sea System. Volume II: Water Column and Interacting with It Atmosphere, Cryosphere, River Runoff and Biosphere*; Lisitzin, A.P., Nemirovskaya, I.A., Eds.; Scientific World: Moscow, Russia, 2012; pp. 19–48. (In Russian)
49. Deryugin, K.M. Fauna of the White Sea and the conditions of its existence. *Res. Seas USSR* **1928**, *7–8*, 511. (In Russian)
50. Locarnini, R.A.; Mishonov, A.V.; Antonov, J.I.; Boyer, T.P.; Garcia, H.E.; Baranova, O.K.; Zweng, M.M.; Paver, C.R.; Reagan, J.R.; Johnson, D.R.; et al. World Ocean Atlas 2013, Volume 1: Temperature. In *NOAA Atlas NESDIS 73*; Levitus, S., Mishonov, A., Eds.; U.S. Department of Commerce, National Oceanic and Atmospheric Administration: Silver Spring, MD, USA, 2013; p. 40.
51. Zweng, M.M.; Reagan, J.R.; Antonov, J.I.; Locarnini, R.A.; Mishonov, A.V.; Boyer, T.P.; Garcia, H.E.; Baranova, O.K.; Johnson, D.R.; Seidov, D.; et al. World Ocean Atlas 2013, Volume 2: Salinity. In *NOAA Atlas NESDIS 74*; Levitus, S., Mishonov, A., Eds.; U.S. Department of Commerce, National Oceanic and Atmospheric Administration: Silver Spring, MD, USA, 2013; 39p.
52. Petelin, V.P. *Grain-Size Analysis of Sea Bottom Sediments*; Nauka: Moscow, USSR, 1967; p. 128. (In Russian)
53. Alekseeva, T.N.; Sval'nov, V.N. Grain-Size Parameters of Marine Sediments. *Oceanology* **2006**, *46*, 430–439. [CrossRef]
54. Bezrukov, I.L.; Lisitsyn, A.P. Classification of the sediments of modern marine ponds. *Proc. Inst. Oceanol. USSR Acad. Sci.* **1960**, *32*, 313. (In Russian)
55. Blaauw, M.; Christen, A. Flexible Paleoclimate Age-Depth Models Using an Autoregressive Gamma Process. *Bayesian Anal.* **2011**, *6*, 457–474. [CrossRef]
56. Heaton, T.J.; Köhler, P.; Butzin, M.; Bard, E.; Reimer, R.W.; Austin, W.E.N.; Bronk Ramsey, C.; Grootes, P.M.; Hughen, K.A.; Kromer, B.; et al. Marine20 - The Marine Radiocarbon Age Calibration Curve (0–55,000 Cal BP). *Radiocarbon* **2020**, *62*, 779–820. [CrossRef]
57. Bevington, P.R. *Data Reduction and Error Analysis for the Physical Sciences*; McGraw-Hill: New York, NY, USA, 1969; p. 336.
58. Zaretskaya, N.E.; Maksimov, F.E.; Khaitov, V.M.; Shevchenko, N.V.; Kuznetsov, V.J.; Pokrovskiy, B.G. Interdisciplinary studies of the White Sea reservoir effect. In *Geology of Seas and Oceans: Proceedings of XX International Conference on Marine Geology*; Lisitzin, A.P., Politova, N.V., Shevchenko, V.P., Eds.; GEOS: Moscow, Russia, 2013; Volume 3, pp. 165–169. (In Russian)
59. Hadden, C.S.; Hutchinson, I.; Martindale, A. Dating Marine Shell: A Guide for the Wary North American Archaeologist. *Am. Antiq.* **2023**, *88*, 62–78. [CrossRef]
60. Brice, C.; de Vernal, A.; Ivanova, E.; van Bellen, S.; Van Nieuwenhove, N. Palynological evidence of sea-surface conditions in the Barents Sea off northeast Svalbard during the postglacial period. *Quat. Res.* **2020**, *108*, 180–194. [CrossRef]
61. *Diatoms of the USSR (Fossil and Modern)*; Nauka: Leningrad, USSR, 1974; Volume 1, p. 403. (In Russian)
62. Battarbee, R.W. A new method for estimation of absolute microfossil numbers, with reference especially to diatoms. *Limnol. Oceanogr.* **1973**, *18*, 647–653. [CrossRef]
63. Zabelina, M.M.; Kiselev, I.A.; Proshkina-Lavrenko, A.I.; Sheshukova, V.S. *Identification Book of Freshwater Algae of the USSR. Iss. 4. Diatom Algae*; Soviet Science: Moscow, USSR, 1951; p. 619. (In Russian)
64. *Diatoms of the USSR (Fossil and Modern)*; Nauka: Leningrad, USSR, 1988; Volume 2.1, p. 116. (In Russian)
65. *Diatoms of the USSR (Fossil and Recent)*; Nauka: St. Petersburg, Russia, 1992; Volume 2.2, p. 125. (In Russian)
66. Diatoms of Russia and Adjacent Countries. *Fossil and Recent*; St. Peterburg Gos. Univ.: St. Petersburg, Russia, 2002; Volume 2.3, p. 112. (In Russian)
67. Diatoms of Russia and Adjacent Countries. *Fossil and Recent*; St. Peterburg Gos. Univ.: St. Petersburg, Russia, 2006; Volume 2.4, p. 180. (In Russian)
68. *Algae: A Handbook*; Naukova Dymka: Kyiv, USSR, 1989; p. 608.
69. Hartley, B.; Barber, H.G.; Carter, J.R. *An Atlas of British Diatoms*; Biopress Ltd.: Bristol, UK, 1996; p. 601.
70. Krammer, K. *Diatom of Europe: Diatoms of the European Inland Waters and Comparable Habitats*; Lange-Bertalot, H., Ed.; A.R.G. Gantner Verlag, K.G.: Ruggell, Liechtenstein, 2002; Volume 3, p. 584.
71. Krammer, K. *Diatoms of Europe: Diatoms of the European Inland Waters and Comparable Habitats*; Lange-Bertalot, H., Ed.; A.R.G. Gantner Verlag K.G.: Ruggell, Liechtenstein, 2003; Volume 4, p. 584.
72. Lange-Bertalot, H. *Diatoms of Europe: Diatoms of the European Inland Waters and Comparable Habitats*; A.R.G. Gantner Verlag K.G.: Ruggell, Liechtenstei, 2001; Volume 2, 526p.
73. Polyakova, Y.I. Diatom assemblages in the surface sediments of the Kara Sea (Siberian Arctic) and their relationship to oceanological conditions. In *Siberian River Run-Off in the Kara Sea: Characterization, Quantification, Variability, and Environmental Significance. Proceedings in Marine Sciences*; Stein, R., Fahl, K., Fütterer, D.K., Galimov, E.M., Stepanets, O.V., Eds.; Elsevier: Amsterdam, The Netherlands, 2003; pp. 375–400. [CrossRef]
74. Barinova, S.S.; Medvedeva, L.A.; Anisimova, O.V. *Biodiversity of Algae—Indicators of the Environment*; Pilies Studio: Tel Aviv, Israel, 2006; 498p. (In Russian)
75. Guiry, M.D.; Guiry, G.M. AlgaeBase. World-Wide Electronic Publication, National University of Ireland, Galway. 2022. Available online: http://www.algaebase.org (accessed on 4 November 2022).
76. Spaulding, S.A.; Potapova, M.; Bishop, I.W.; Lee, S.; Gasperak, T.; Jovanovska, E.; Furey, P.C.; Edlund, M.B. Diatoms.org: Supporting taxonomists, connecting communities. *Diatom Res.* **2021**, *4*, 291–304. [CrossRef]

77. Campeau, S.; Pienitz, R.; Hequette, A. Diatoms from the Beaufort Sea coast, southern Arctic Ocean (Canada). Modern analogues for reconstructing Late Quaternary environments and relative sea levels. *Bibl. Diatomol. Band.* **1999**, *41*, 1–244.
78. Kolbe, R.W. Zur Ökologie, Morphologie und Systematik der Brackwasser Diatomeen. *Pflancenforschung* **1927**, *7*, 1–146.
79. Pankow, H. *Ostsee-Algenflora*; Gustav Fischer Verlag: Jena, Germany, 1990; p. 648.
80. Simonsen, R. Untersuchungen zur Systematik und Okologie der Bodendiatomeen der westlichen Ostsee. *Int. Gesanten Hydrobiol. Syst. Beih.* **1962**, *1*, 9–148.
81. Jousé, A.P. *Stratigraphic and paleogeographic studies in the northeastern Pacific Ocean*; Publishing House of the USSR Academy of Sciences: Moscow, Russia, 1962; pp. 1017–1028. (In Russian)
82. Semina, G.I. *Phytoplankton of the Pacific Ocean*; Nauka: Moscow, USSR, 1974; p. 239. (In Russian)
83. Polyakova, Y.I.; Novichkova, Y.A.; Klyuvitkina, T.S. Diatoms and palynomorphs in surface sediments of the Arctic seas and their significance for paleoceanological studies at high latitudes. In *The White Sea System. Volume IV: The Processes of Sedimentation, Geology and History*; Lisitzin, A.P., Shevchenko, V.P., Vorontsova, V.G., Eds.; Scientific World: Moscow, Russia, 2017; pp. 796–859. (In Russian)
84. Polyakova, Y.I. Diatoms of Arctic seas of the USSR and their significance in the study of bottom sediments. *Oceanology* **1988**, *28*, 221–225.
85. Polyakova, Y.I. *The Eurasian Arctic seas during the late Cenozoic*; Scientific World: Moscow, Russia, 1997; p. 146. (In Russian)
86. Beklemishev, K.B.; Semina, G.I. Geography of plankton diatoms of high and moderate latitudes of the world ocean. *Proc. All-Union Hydrobiol. Soc.* **1986**, *27*, 7–23. (In Russian)
87. Makarova, I.V. The genus Thalassiosira in the seas of the USSR. *Proc. Zool. Inst. Acad. Sci. USSR* **1987**, *172*, 26–38. (In Russian)
88. Usachev, P.I. Microflora of polar ice. *Proc. Oceanol. Inst. USSR Acad. Sci.* **1949**, 216–259. (In Russian)
89. Horner, R. Arctic sea-ice biota. In *The Arctic Seas. Climatology, Oceanography. Geology, and Biology*; Herman, Y., Ed.; Springer: Boston, MA, USA, 1989; pp. 123–146.
90. Syvertsen, E.E. Ice algae in the Barents Sea: Types of assemblages, origin, fate and role in the ice-edge phytoplankton bloom. *Polar Res.* **1991**, *10*, 277–287. [CrossRef]
91. von Quillfeldt, C.H. Distribution of diatoms in the Northern Water Polynya, Greenland. *J. Mar. Syst.* **1997**, *10*, 211–240. [CrossRef]
92. Polyakova, Y.I.; Novichkova, E.A.; Agafonova, E.A. Diatoms and aquatic palynomorphs in the bottom sediments of the Barents Sea: Main patterns of distribution and use in paleooceanological studies. In *System of the Barents Sea*; Lisitzin, A.P., Ed.; GEOS: Moscow, Russia, 2021; pp. 64–95, (In Russian). [CrossRef]
93. Lisitzin, A.P. Marginal filter in the oceans. *Oceanology* **1995**, *34*, 671–682.
94. Klyuvitkina, T.S.; Novichkova, E.A. Laboratory processing in the aquatic palynomorph analysis: Problems and solutions. *Oceanology* **2022**, *62*, 270–277. [CrossRef]
95. Zonneveld, K.A.F.; Versteegh, G.; Kodrans-Nsiah, M. Preservation and organic chemistry of Late Cenozoic organic-walled dinoflagellate cysts: A review. *Mar. Micropaleontol.* **2008**, *68*, 179–197. [CrossRef]
96. Rochon, A.; de Vernal, A.; Turon, J.-L.; Matthiessen, J.; Head, M.J. Distribution of recent dinoflagellate cysts in surface sediments from the North Atlantic and adjacent seas in relation to of sea-surface parameters. *Am. Assoc. Stratigr. Palynol. Contrib. Ser.* **1999**, *35*, 146.
97. De Vernal, A.; Henry, M.; Matthiessen, J.; Mudie, P.J.; Rochon, A.; Boessenkool, K.P.; Eynaud, F.; Grøsfjeld, K.; Guiot, J.; Hamel, D.; et al. Dinoflagellate cyst assemblages as tracers of sea-surface conditions in the northern North Atlantic, Arctic and sub-Arctic seas: The new 'n = 677' data base and its application for quantitative palaeoceanographic reconstruction. *J. Quat. Sci.* **2001**, *16*, 681–698. [CrossRef]
98. Head, M.J.; Harland, R.; Matthiessen, J. Cold marine indicators of the late Quaternary: The new dinoflagellate cyst genus Islandinium and related morphotypes. *J. Quat. Sci.* **2001**, *16*, 621–636. [CrossRef]
99. Van Nieuwenhove, N.; Head, M.J.; Limoges, A.; Pospelova, V.; Mertens, K.; Matthiessen, J.; De Schepper, S.; de Vernal, A.; Eynaud, F.; Londeix, L.; et al. An overview and brief description of common marine organic-walled dinoflagellate cyst taxa occurring in surface sediments of the Northern Hemisphere. *Mar. Micropaleontol.* **2020**, *159*, 101814. [CrossRef]
100. Mertens, K.N.; Gu, H.; Gurdebeke, P.R.; Takano, Y.; Clarke, D.; Aydin, H.; Li, Z.; Pospelova, V.; Shin, H.; Li, Z.; et al. A review of rare, poorly known, and morphologically problematic extant marine organic-walled dinoflagellate cyst taxa of the orders Gymnodiniales and Peridiniales from the Northern Hemisphere. *Mar. Micropaleontol.* **2020**, *159*, 101773. [CrossRef]
101. Kupriyanova, L.A.; Aleshina, L.A. *Pollen and Spores of Flora of the European Part of the USSR*; Science: Leningrad, USSR, 1972; Volume 1, p. 171. (In Russian)
102. Kupriyanova, L.A.; Aleshina, L.A. *Pollen of Dicotyledonous Plants of the Flora of the European Part of the USSR. Lamiaceae=Zygophyllaceae*; Science: Leningrad, USSR, 1978; p. 183. (In Russian)
103. Kupriyanova, L.A. *Palynology of the Catkins*; Science: Moscow–Leningrad, Russia, 1965; p. 215.
104. Reille, M. *Pollen et Spores d'Europe et d'Afrique du Nord*; Laboratoire de botanique historique et palynologie: Marseille, France, 1992; p. 520.
105. Stockmarr, J. Tables with spores used in absolute pollen analysis. *Pollen Spores* **1971**, *13*, 616–621.
106. De Vernal, A.; Rochon, A.; Fréchette, B.; Henry, M.; Radi, T.; Solignac, S. Reconstructing past sea ice cover of the northern hemisphere from dinocyst assemblages: Status of the approach. *Quat. Sci. Rev.* **2013**, *79*, 122–134. [CrossRef]

107. De Vernal, A.; Radi, T.; Zaragosi, S.; Van Nieuwenhove, N.; Rochon, A.; Allan, E.; De Schepper, S.; Eynaud, F.; Head, M.; Limoges, A.; et al. Distribution of common modern dinoflagellate cyst taxa in surface sediments of the Northern Hemisphere in relation to environmental parameters: The new n = 1968 database. *Marine Micropaleontology* **2020**, *159*, 101796. [CrossRef]
108. Belyaev, N.A.; Ponyaev, M.S.; Kiriutin, A.M. Organic carbon in water, particulate matter, and upper layer of bottom sediments of the central part of the Kara Sea. *Oceanology* **2015**, *55*, 508–520. [CrossRef]
109. Lein, A.; Novichkova, E.; Rybalko, A.; Ivanov, M. Carbon isotope composition of organic matter in Holocene sediments of the White Sea as one of the indicators of sedimentation conditions. *Dokl. Earth Sci.* **2013**, *452*, 1056–1061. [CrossRef]
110. Zong, Y. Implications of *Paralia sulcata* abundance in Scottish isolation basins. *Diatom Res.* **1997**, *12*, 125–150. [CrossRef]
111. Georgiev, A.A. Epiphytic Diatoms of Macrophytes of the Velikaya Salma Strait (Kandalaksha Bay, the White Sea). Ph.D. Thesis, MSU, Moscow, Russia, 2010; p. 23. (In Russian).
112. Grøsfjeld, K.; Harland, R.; Howe, J. Dinoflagellate cyst assemblages inshore and off shore Svalbard reflecting their modern hydrography and climate. *Nor. J. Geol.* **2009**, *89*, 121–132.
113. Solignac, S.; Grøsfjeld, K.; Giraudeau, J.; de Vernal, A.; Gade, H. Distribution of recent dinocyst assemblages in the western Barents Sea. *Nor. J. Geol.* **2009**, *89*, 109–119.
114. Matthiessen, J.; de Vernal, A.; Head, M.; Okolodkov, Y.; Angel, P.; Zonneveld, K.; Harland, R. Modern organic walled dinoflagellate cysts in Arctic marine environments and their (paleo-) environmental significance. *Paläontologische Z.* **2005**, *79*, 3–51. [CrossRef]
115. Matthiessen, J.; Schreck, M.; De Schepper, S.; Coralie, Z.; de Vernal, A. Quaternary dinoflagellate cysts in the Arctic Ocean: Potential and limitations for stratigraphy and paleoenvironmental reconstructions. *Quat. Sci. Rev.* **2018**, *192*, 1–26. [CrossRef]
116. Zonneveld, K.A.F.; Marret, F.; Versteegh, G.J.M.; Bogus, K. Atlas of modern dinoflagellate cyst distribution based on 2405 data points. *Rev. Palaeobot. Palynol.* **2013**, *191*, 1–197. [CrossRef]
117. Bonnet, S.; de Vernal, A.; Hillaire-Marcel, C.; Radi, T.; Husum, K. Variability of sea-surface temperature and sea-ice cover in the Fram Strait over the last two millennia. *Mar. Micropaleontol.* **2010**, *74*, 59–74. [CrossRef]
118. Wang, L.; Rioual, P.; Panizzo, V.N.; Lu, H.; Gu, Z.; Chu, G.; Yang, D.; Han, J.; Liu, J.; Mackay, A.W. A 1000-yr record of environmental change in NE China indicated by diatom assemblages from maar lake Erlongwan. *Quat. Res.* **2012**, *78*, 24–34. [CrossRef]
119. Wang, L.; Mackay, A.W.; Leng, M.J.; Rioual, P.; Panizzo, V.; Lu, H.; Chu, G.; Han, J.; Kendrick, C. Influence of the ratio of planktonic to benthic diatoms on lacustrine organic matter d13C from Erlongwan maar lake, northeast China. *Org. Geochem.* **2013**, *54*, 62–68. [CrossRef]
120. Zhang, J.; Witkowski, A.; Tomczak, M.; Li, C.; McCartney, K.; Xia, Z. The sub-fossil diatom distribution in the Beibu Gulf (northwest South China Sea) and related environmental interpretation. *PeerJ.* **2022**, *10*, e13115. [CrossRef]
121. Lastochkin, A.N. Bottom relief of the Kara Sea. *Geomorphologiya* **1977**, *2*, 84–91. (In Russian)
122. Pavlidis, Y.; Ionin, A.S.; Shcherbakov, F.A.; Dunaev, N.N.; Nikiforov, S.L. *Arctic Shelf. Late Quaternary History as the Basis for the Development Forecast*; GEOS: Moscow, Russia, 1998; p. 187. (In Russian)
123. Gusev, E.A.; Andreeva, I.A.; Anikina, N.Y.; Bondarenko, S.A.; Derevyanko, L.G.; Iosifidi, A.G.; Klyuvitkina, T.S.; Litvinenko, I.V.; Petrova, V.I.; Polyakova, E.I.; et al. Stratigraphy of Late Cenozoic sediments of the western Churchi Sea: New results from shallow drilling and seismic-reflection profiling. *Glob. Planet. Change* **2009**, *68*, 115–131. [CrossRef]
124. Makarov, A.S.; Bolshiyanov, D.Y. Variability of the sea level of the Russian Arctic in the Holocene. Coastal zone—A look into the future. In Proceedings of the XXV International Coastal Conference, Seoul, Republic of Korea, 15–20 June 2014; Volume 2, pp. 34–36. (In Russian).
125. Lambeck, K.; Chappell, J. Sea Level Change Through the Last Glacial Cycle. *Science* **2001**, *292*, 679–686. [CrossRef]
126. Lavrova, M.A. The main stages of the Quaternary history of the Kola Peninsula. *News All-Union Geogr. Soc.* **1947**, *79*, 21–38.
127. Kolka, V.V.; Evzerov, V.Y.; Möller, J.; Korner, D. Postglacial glacioisostatic movements in the northeast of the Baltic Shield. In *New Data on Geology and Minerals of the Kola Peninsula*; Publishing House of the Kola Science Center RAS: Apatity, Russia, 2005; pp. 15–25. (In Russian)
128. Kolka, V.V.; Korsakova, O.P.; Shelekhova, T.S.; Lavrova, N.B.; Arslanov, K.A. Reconstruction of the Relative Level of the White Sea during the Holocene on the Karelian Coast near Engozero Settlement, Northern Karelia. *Dokl. Earth Sci.* **2013**, *449*, 434–438. [CrossRef]
129. Romanenko, F.A.; Shilova, O.S. The postglacial uplift of the Karelian coast of the White Sea according to radiocarbon and diatom analyses of lacustrine-boggy deposits of Kindo peninsula. *Dokl. Earth Sci.* **2012**, *442*, 242–246. [CrossRef]
130. Zaretskaya, N.E.; Repkina, T.Y. New data on the history of the Tersky coast of the White Sea in the Holocene (the region of the mouth of the Varzuga river). In *Geology of Seas and Oceans, Proceedings of the XXI International Scientific Conference (School) on Marine Geology*; GEOS: Moscow, Russia, 2015; Volume 3, pp. 185–189.
131. Subetto, D.A.; Shevchenko, V.P.; Ludikova, A.V.; Kuznetsov, D.D.; Sapelko, T.V.; Lisitsyn, A.P.; Evzerov, V.Y.; van Beek, P.; Souhaut, M.; Subetto, G.D. Chronology of isolation of lakes in the Solovetsky Archipelago and rates of present-day lacustrine sedimentation. *Dokl. Earth Sci.* **2012**, *446*, 1042–1048. [CrossRef]
132. Baranskaya, A.; Khan, N.; Romanenko, F.; Roy, K.; Peltier, W.R.; Horton, B. A postglacial relative sea-level database for the Russian Arctic coast. *Quat. Sci. Rev.* **2018**, *199*, 188–205. [CrossRef]
133. Nikolaeva, S.B. Postglacial tectonics and paleoseismodislocations in the Kovda region (Kandalaksha Bay, eastern part of the Fennoscandian shield). *Bull. St.-Petersb. Univ. Earth Sci.* **2019**, *64*, 434–453. [CrossRef]

134. Nikonov, A.A.; Shvarev, S.V. Strong earthquakes in the Russian part of the Fennoscandian shield over the past 13 thousand years. *GeoInfo* **2019**, *1*.
135. Avenarius, I.G. Morphostructure of the White Sea region. *Geomorphology* **2004**, *3*, 48–56. (In Russian) [CrossRef]
136. Zykov, D.S.; Kolodyazhny, S.Y.; Baluev, A.S. Signs of horizontal neotectonic mobility of the basement in the White Sea region. *Bullyuten MOIP. Dep. Geol.* **2008**, *83*, 15–25. (In Russian)
137. Zaretskaya, N.; Panin, A.; Karpukhina, N. The SIS limits and related proglacial events in the Severnaya Dvina basin, Northwestern Russia: Review and new data. *Bull. Geol. Soc. Finl.* **2018**, *90*, 301–313. [CrossRef]
138. Rigual-Hernández, A.S.; Colmenero-Hidalgo, E.; Martrat, B.; Bárcena, M.A.; de Vernal, A.; Sierro, F.J.; Flores, J.A.; Grimalt, J.O.; Henry, M.; Lucchi, R.G. Svalbard ice-sheet decay after the Last Glacial Maximum: New insights from micropalaeontological and organic biomarker paleoceanographical reconstructions. *Palaeogeogr. Palaeoclimat. Palaeoecol.* **2017**, *465*, 225–236. [CrossRef]
139. Polyakova, Y.I.; Bauch, H.A.; Klyuvitkina, T.S. Early to Middle Holocene changes in Laptev Sea water masses deduced from diatom and aquatic palynomorph assemblages. *Glob. Planet. Change* **2005**, *48*, 208–222. [CrossRef]
140. Duplessy, J.C.; Cortijo, E.; Ivanova, E.; Khusid, T.; Labeyrie, L.; Levitan, M.; Murdmaa, I.; Paterne, M. Paleoceanography of the Barents Sea during the Holocene. *Paleoceanography* **2005**, *20*, PA4004. [CrossRef]
141. Chernov, A.V.; Zaretskaya, N.E.; Panin, A.V. Evolution and dynamics of upper and middle Vychegda in Holocene. *Izv. RGO* **2015**, *147*, 27–49.
142. Zaretskaya, N.E.; Shevchenko, N.V.; Khaitov, V.M. Holocene taphocenoses of the White Sea malacofauna: Features of formation and radiocarbon chronology. Proceeding of the Third Russian Scientific Conference with International Participation "The Dynamics of Modern Ecosystems in the Holocene", Kazan, Tatarstan Republik, Russia, 12–15 March 2013; pp. 160–164. (In Russian).
143. Kolka, V.V.; Korsakova, O.P. The position of the White Sea coastline and neotectonic movements in the northeast of Fennoscandia in the Late Glacial and Holocene. In *The White Sea System. Volume IV: The Processes of Sedimentation, Geology and History*; Lisitzin, A.P., Shevchenko, V.P., Vorontsova, V.G., Eds.; Scientific World: Moscow, Russia, 2017; pp. 222–249. (In Russian)
144. Sidorchuk, A.Y.; Borisova, O.K.; Kovalyukh, N.N.; Panin, A.V.; Chernov, A.V. Paleohydrology of the Lower Vychegda in the Late Glacial and Holocene. *Vestn. Mosk. Univ. Ser. 5 Geogr.* **1999**, *5*, 34–41. (In Russian)
145. Sidorchuk, A.Y.; Panin, A.V.; Borisova, O.K. Decreased runoff of rivers in the northern Eurasian plains during the Holocene optimum. *Water Resour.* **2012**, *39*, 1–14. (In Russian) [CrossRef]